MUSCLE BIOLOGY

Activation of mTORC1 in skeletal muscle regulates whole-body metabolism through FGF21

Maitea Guridi,[1] Lionel A. Tintignac,[1,2] Shuo Lin,[1] Barbara Kupr,[1] Perrine Castets,[1,3] Markus A. Rüegg[1]*

Skeletal muscle is the largest organ, comprising 40% of the total body lean mass, and affects whole-body metabolism in multiple ways. We investigated the signaling pathways involved in this process using TSCmKO mice, which have a skeletal muscle–specific depletion of TSC1 (tuberous sclerosis complex 1). This deficiency results in the constitutive activation of mammalian target of rapamycin complex 1 (mTORC1), which enhances cell growth by promoting protein synthesis. TSCmKO mice were lean, with increased insulin sensitivity, as well as changes in white and brown adipose tissue and liver indicative of increased fatty acid oxidation. These differences were due to increased plasma concentrations of fibroblast growth factor 21 (FGF21), a hormone that stimulates glucose uptake and fatty acid oxidation. The skeletal muscle of TSCmKO mice released FGF21 because of mTORC1-triggered endoplasmic reticulum (ER) stress and activation of a pathway involving PERK (protein kinase RNA-like ER kinase), eIF2α (eukaryotic translation initiation factor 2α), and ATF4 (activating transcription factor 4). Treatment of TSCmKO mice with a chemical chaperone that alleviates ER stress reduced FGF21 production in muscle and increased body weight. Moreover, injection of function-blocking antibodies directed against FGF21 largely normalized the metabolic phenotype of the mice. Thus, sustained activation of mTORC1 signaling in skeletal muscle regulated whole-body metabolism through the induction of FGF21, which, over the long term, caused severe lipodystrophy.

INTRODUCTION

Skeletal muscle is a dynamic tissue with a key role in the maintenance of metabolic homeostasis. Several lines of evidence indicate that alterations of the normal muscle function, as for example in muscular dystrophies, obesity or diabetes, can affect the metabolism at the whole-body level (*1*, *2*). The effect of muscle on the global metabolism has been linked to the discovery of specific cytokines secreted by the muscle, called myokines, which exert effects on angiogenesis, myogenesis, and energy metabolism (*3*). Specifically, fibroblast growth factor 21 (FGF21) is secreted by skeletal muscle and protects from diet-induced obesity and insulin resistance (*4*). FGF21 is a member of an atypical subfamily of FGFs that is released into the circulation because of the lack of a heparin-binding domain and thus acts as an endocrine factor (*5*). FGF21 is at the center of extensive research as a target molecule to treat metabolic disorders, such as diabetes and obesity (*6*). FGF21 promotes weight loss through an increase in fatty acid oxidation and lowers triglyceridemia and decreases glycemia by improving insulin sensitivity (*7*). Transgenic mice overexpressing FGF21 in the liver are protected against diet-induced obesity (*8*), and FGF21 pharmacotherapy in diabetic and obese mice rapidly improves metabolic abnormalities (*9*, *10*). FGF21 is primarily synthesized in the liver upon starvation or a high-fat diet (HFD) and can also be induced in adipose tissue (*11*, *12*). In skeletal muscle, FGF21 is secreted in response to the activation of cellular stress pathways, such as autophagy impairment and/or mitochondrial dysfunction (*4*, *13*).

The mammalian target of rapamycin (mTOR) is a master regulator of metabolic homeostasis, and its deregulation is associated with metabolic disorders, such as obesity and diabetes. mTOR is an atypical serine/threonine protein kinase that senses nutrient availability and cellular energy status to promote anabolic processes (*14*). mTOR assembles into two distinct multiprotein complexes: mTOR complex 1 (mTORC1), which promotes cell growth through the regulation of protein synthesis, and mTORC2, which regulates cytoskeleton organization. Development of transgenic mouse models deficient for components of mTORC1 or mTORC2 in metabolic organs, such as adipose tissue or liver, has shown that these complexes play essential roles in glucose and lipid homeostasis (*15*, *16*). We have previously shown that mice with muscle-specific depletion of raptor (RAmKO mice), an essential component of mTORC1, develop a progressive myopathy (*17*). Surprisingly, mice with muscle-specific depletion of the mTORC1 inhibitor TSC1 (TSCmKO mice), characterized by sustained mTORC1 activation and increased protein synthesis, also develop a late-onset myopathy (*18*) with a marked atrophy of most muscles (*19*). These alterations in TSCmKO muscle are related to increased proteasome activity and to the blockade of autophagy induction (*18*, *19*). Concomitant with the myopathy, TSCmKO mice show decreased fat mass (*18*), suggesting that constitutive mTORC1 activation in skeletal muscle may exert endocrine effects on nonmuscle tissues. In addition, RAmKO mice and mice deficient for mTOR in skeletal muscle have altered glucose metabolism (*17*, *20*), pointing to a possible role of muscle mTORC1 signaling in the regulation of whole-body metabolism.

Here, we examined the global metabolic changes in TSCmKO mice starting at a young age and showed that they were resistant to obesity and developed a severe lipodystrophy with age. The constitutive activation of mTORC1 in muscle led to an increased FGF21 synthesis and higher concentration of FGF21 in plasma. This was largely due to the endoplasmic reticulum (ER) stress–activated PERK (protein kinase RNA-like ER kinase)–eIF2α (eukaryotic translation initiation factor 2α)–ATF4 (activating transcription factor 4) pathway. Thus, we showed that specific perturbation of mTORC1 signaling in muscle modified whole-body homeostasis by inducing release of FGF21 as a myokine.

[1]Biozentrum, University of Basel, CH-4056 Basel, Switzerland. [2]INRA, UMR866, Université Montpellier 1, Université Montpellier 2, 34090 Montpellier, France. [3]Neuromuscular Research Center, Departments of Neurology and Biomedicine, Pharmazentrum, Basel University Hospital, 4056 Basel, Switzerland.
*Corresponding author. E-mail: markus-a.ruegg@unibas.ch

RESULTS

mTORC1 activation in skeletal muscle promotes a lean phenotype

In TSCmKO mice, mTORC1 is constitutively activated in skeletal muscle, and they develop a late-onset myopathy in conjunction with a reduced body weight resulting from the loss of both fat and lean mass (*18*). To determine if these differences in body mass were a consequence of the myopathy, we analyzed the progression of the metabolic phenotype of TSCmKO mice, starting at the age of 10 weeks when the mice are healthy with no signs of myopathy (fig. S1A). At this young age, TSCmKO mice were 15% lighter than control mice, and this difference increased to 31% at 40 weeks of age (Fig. 1A and table S1). We also noticed that the tibia length was slightly but significantly reduced in TSCmKO mice compared to age-matched control mice (table S1), suggesting a difference in overall growth. Analysis of plasma revealed no changes in growth hormone (GH) concentrations (fig. S1B) but a significant decrease in insulin-like growth factor 1 (IGF-1) (Fig. 1B), which could correlate with the reduced growth (*21*). Whereas

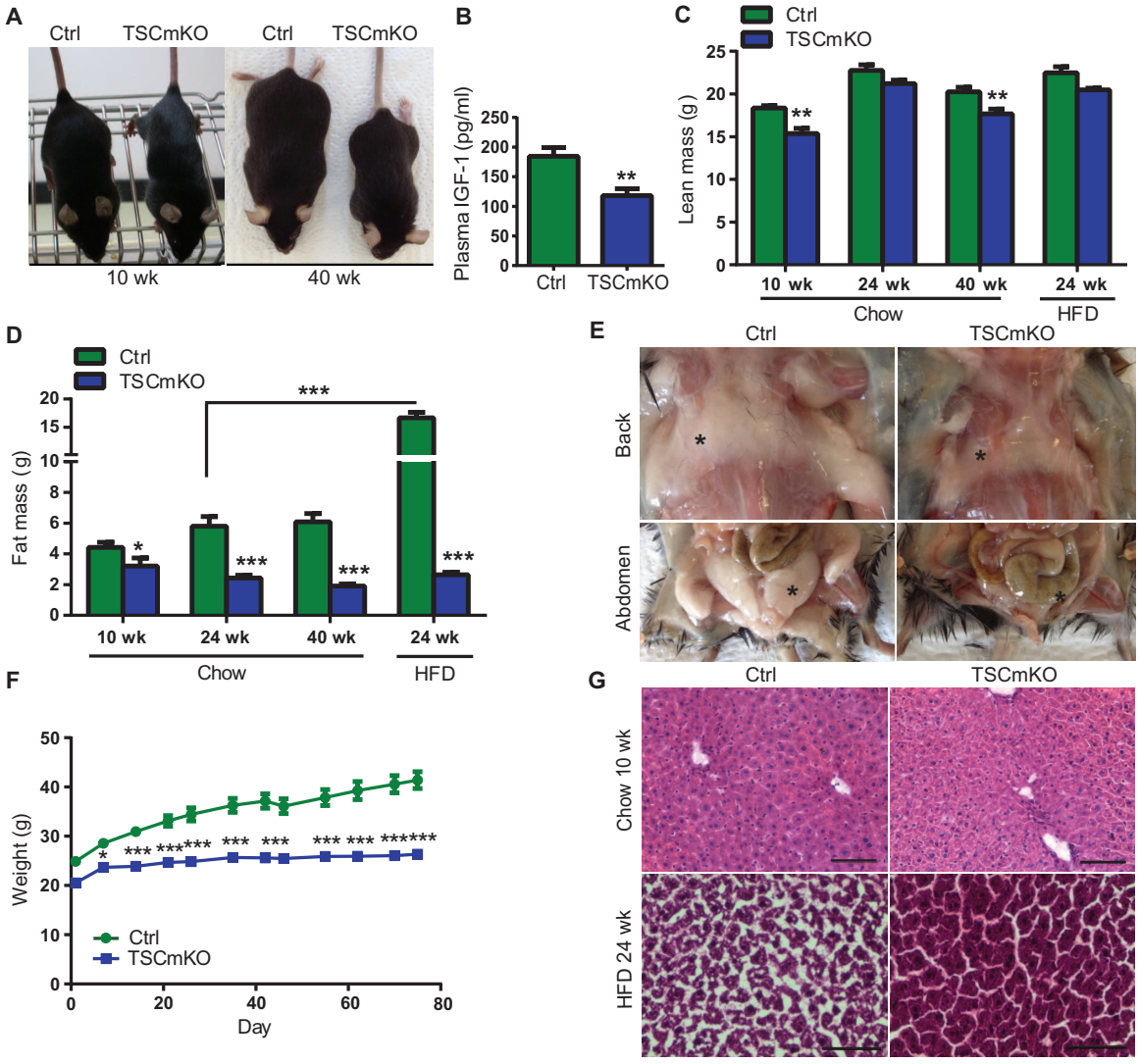

Fig. 1. TSCmKO mice show a decreased body mass and are resistant to HFD. (**A**) Pictures of 10- and 40-week-old TSCmKO and control (Ctrl) littermates. (**B**) Plasma IGF-1 concentrations were decreased in 12-week-old TSCmKO mice compared to control littermates (n = 7 mice per genotype). (**C** and **D**) Echo-MRI analysis revealed decreased lean mass (C) and fat mass (D) in TSCmKO mice at 10 (n = 8 mice per genotype), 24 (n = 7 mice per genotype), and 40 (n = 8 mice per genotype) weeks of age under a chow diet and at 24 weeks of age with the HFD (n = 6 mice per genotype). (**E**) Subscapular-subcutaneous (Back) and inguinal-perigonadal (Abdomen) fat deposits from 40-week-old control and TSCmKO mice. Asterisks point at fat depots. Images are representative of nine mice per genotype. (**F**) Weekly weight measurement during 14 weeks of HFD showed the inability of TSCmKO mice to gain weight (n = 6 mice per genotype). Linear regression analysis showed that the two groups differ significantly (P < 0.001). (**G**) Hematoxylin and eosin (H&E) staining showed normal liver histology in 10-week-old TSCmKO and control mice on a chow diet. After 14 weeks of HFD, control mice, but not TSCmKO mice, showed hepatic steatosis. Images are representative of four sections from three mice per genotype and condition. Scale bars, 100 μm. Data represent means ± SEM; *P < 0.05, **P < 0.01, ***P < 0.001.

the difference in tibia length between TSCmKO and control mice remained constant between 10 and 40 weeks of age, the weight difference was progressive and increased with age (table S1).

The activity and the feeding behavior of the mutant and control mice were similar (fig. S1, C to F). Lean mass was reduced in TSCmKO mice but followed the same pattern with age as in control mice (Fig. 1C). In contrast, the loss in fat mass in TSCmKO mice increased with age (Fig. 1, D and E). The difference in fat mass between control and TSCmKO mice was exaggerated by placing the mice on a 14-week-long HFD, starting at the age of 10 weeks. As expected, the body weight of the control mice progressively increased (Fig. 1F), which was largely due to a gain in fat mass (Fig. 1D), and these mice developed hepatic steatosis (Fig. 1G). In contrast, TSCmKO mice were resistant to these changes (Fig. 1, D, F, and G). Compared to controls, TSCmKO mice ate more and were more active during the HFD (fig. S1, G and H). Together, these results emphasized the inability of mutant mice to gain weight, which was mainly due to a change in fat mass, and they pointed toward a major perturbation of the global metabolism in TSCmKO mice.

TSCmKO mice show an increase in fatty acid oxidation

To further examine the resistance of TSCmKO mice to HFD, we measured energy expenditure. Whereas energy expenditure was similar between 10-week-old control and mutant mice, it was increased in 40-week-old TSCmKO mice and in mutant mice on the HFD (Fig. 2A). The enhanced energy expenditure correlated with increased transcription of *Ucp2* (which encodes uncoupling protein 2) in skeletal muscle (Fig. 2B). Because uncoupling proteins (UCPs) uncouple energy production from oxidative phosphorylation, we also measured adenosine triphosphate (ATP) concentrations and found a significant reduction in TSCmKO skeletal muscle (Fig. 2C). Consistently, in TSCmKO muscle, the phosphorylation (Ser^{173}) and thus activation of the adenosine monophosphate–activated protein kinase (AMPK) were increased (Fig. 2D). Furthermore, the abundance of pyruvate dehydrogenase kinase (PDK4) was increased (Fig. 2D), suggesting that TSCmKO muscle fibers switched to fatty acids as energy substrate. Expression of *Pdk4*, as well as other genes associated with fatty acid oxidation, such as *peroxisome proliferator activated receptor-γ coactivator 1-β* (*Ppargc1b*) and *fatty acid binding protein 3* (*Fabp3*), was increased in TSCmKO muscle (Fig. 2B). The expression of all the genes measured in TSCmKO liver was unchanged (fig. S2A), except for a decrease in *acetyl-CoA carboxylase 1* (*Acac1*), which encodes an enzyme involved in fatty acid synthesis, and an increase in *peroxisome proliferator–activated receptor-γ coactivator 1-α* (*Ppargc1a*), which encodes a transcriptional coactivator that is PGC1α, involved in the control of fatty acid oxidation (*22*) (Fig. 2E). These results suggest that fatty acid oxidation could also be increased in the liver of mutant mice (*23*).

Increased fatty acid oxidation, as observed for example during fasting, induces ketone body synthesis in the liver as an alternative source of energy (*24*). The concentration of β-hydroxybutyrate, which indicates ketone body production, was increased in the plasma of TSCmKO mice compared to controls (Fig. 2F). Moreover, we found increased expression of mRNAs encoding the main enzymes involved in ketone body catabolism, such as D-β-*hydroxybutyrate dehydrogenase 1* (*Bdh1*) and *3-oxoacid-CoA transferase 1* (*Oxct1*), in TSCmKO skeletal muscle, whereas the expression of ketogenic genes *3-hydroxy 3-methylglutaryl-CoA synthase 2* (*Hmgcs2*) and *acetyl-CoA acyltransferase 1* (*Acat1*) was significantly decreased (Fig. 2B). Likewise, OXCT1 protein abundance was significantly increased in mutant muscle (Fig. 2D). These results support the notion that the enhanced fatty acid oxidation caused increased ketogenesis in the liver of TSCmKO mice, which, in turn, led to a higher utilization of ketone bodies in mutant muscle.

Because a global change in fatty acid metabolism would also have an impact on the white adipose tissue (WAT), we analyzed the histology of the subcutaneous-inguinal WAT in 12-week-old control and TSCmKO mice. Mutant mice had smaller multilocular adipocytes (Fig. 2G), also called brite or beige adipocytes, a phenotype suggestive of the "browning" of WAT, a process characterized by increased number of mitochondria and thermogenic capacity (*25*). Furthermore, there were smaller and fewer lipid droplets in the adipocytes of brown adipose tissue (BAT) of the mutant mice (Fig. 2G), indicative of increased fatty acid oxidation. Accordingly, the mRNA and/or protein abundance of PGC1α, carnitine palmitoyltransferase 1 (CPT-I), *Ucp1*, *PR domain containing 16* (*Prdm16*), and *cell death–inducing DFFa-like effector α* (*Cidea*), which are markers for WAT browning and fatty acid oxidation (*22*, *26*), were increased in the WAT of TSCmKO mice (Fig. 2, H and I). Moreover, the phosphorylated, active form of hormone-sensitive lipase (HSL) was increased in WAT from TSCmKO mice (Fig. 2I). Consistent with increased triglyceride breakdown and enhanced fatty acid oxidation, free fatty acid concentration was increased in plasma from starved TSCmKO mice compared to control mice (fig. S2B). However, plasma triglyceride and cholesterol concentrations were unchanged in TSCmKO mice (table S2). We therefore concluded that the increased fatty acid oxidation in WAT, BAT, liver, and muscle, combined with increased ketogenesis in liver, resulted in the progressive loss of fat mass and adipose depots in TSCmKO mice.

TSCmKO mice have increased glucose absorption and improved insulin sensitivity

Next, we examined glucose homeostasis in the mice. Glucose blood concentrations were significantly reduced in TSCmKO mice at 10 and 40 weeks of age and remained significantly lower on the HFD (Fig. 3A). Similarly, plasma insulin concentration was decreased and remained low on the HFD (Fig. 3B). The low concentrations of insulin were unlikely due to a deficiency of the pancreas because its histology (general tissue integrity and presence of Langerhans islets) was similar to that of controls (fig. S3A). Moreover, although insulin concentrations were low in TSCmKO mice under both starved and fed conditions, they were efficiently increased upon glucose administration (Fig. 3C). Additionally, during an insulin tolerance test while on HFD, TSCmKO mice showed improved insulin sensitivity compared to the control mice (Fig. 3D). Another mechanism that regulates plasma glucose concentrations is liver gluconeogenesis. Although we did not detect gluconeogenesis defects in 10-week-old TSCmKO mice when compared to control animals (fig. S3B), gluconeogenesis became impaired in 24-week-old TSCmKO mice as shown by decreased glucose production in a pyruvate tolerance test (Fig. 3E). Hence, these results indicated a general change in glucose metabolism in TSCmKO mice.

We next analyzed the expression of glucose metabolism genes in skeletal muscle. Whereas the expression of most of the genes measured was unchanged (fig. S3C), that of *Slc2a1*, which encodes the glucose transporter GLUT1, was significantly increased in TSCmKO mice (Fig. 3F). Likewise, GLUT1 protein abundance was increased, whereas the amount of GLUT4 remained unchanged in TSCmKO muscle (Fig. 3G). Although TSCmKO muscle did not show changes in the expression of genes encoding enzymes involved in glycolysis (fig. S3C), it contained more glycogen than control muscle (Fig. 3H). As expected, reduced Akt activity in TSCmKO muscle (*19*) led to a significant decrease in the inhibitory phosphorylation (Ser^{9}) of glycogen synthase kinase 3β (GSK3β) (Fig. 3G). However, despite GSK3β being more active, phosphorylation of its target, glycogen synthase (GS), was unchanged in mutant muscle (Fig. 3G) because increased availability of its substrate glucose might counteract the inhibitory activity of GSK3β. Hence, the increase in glucose uptake through GLUT1 under basal

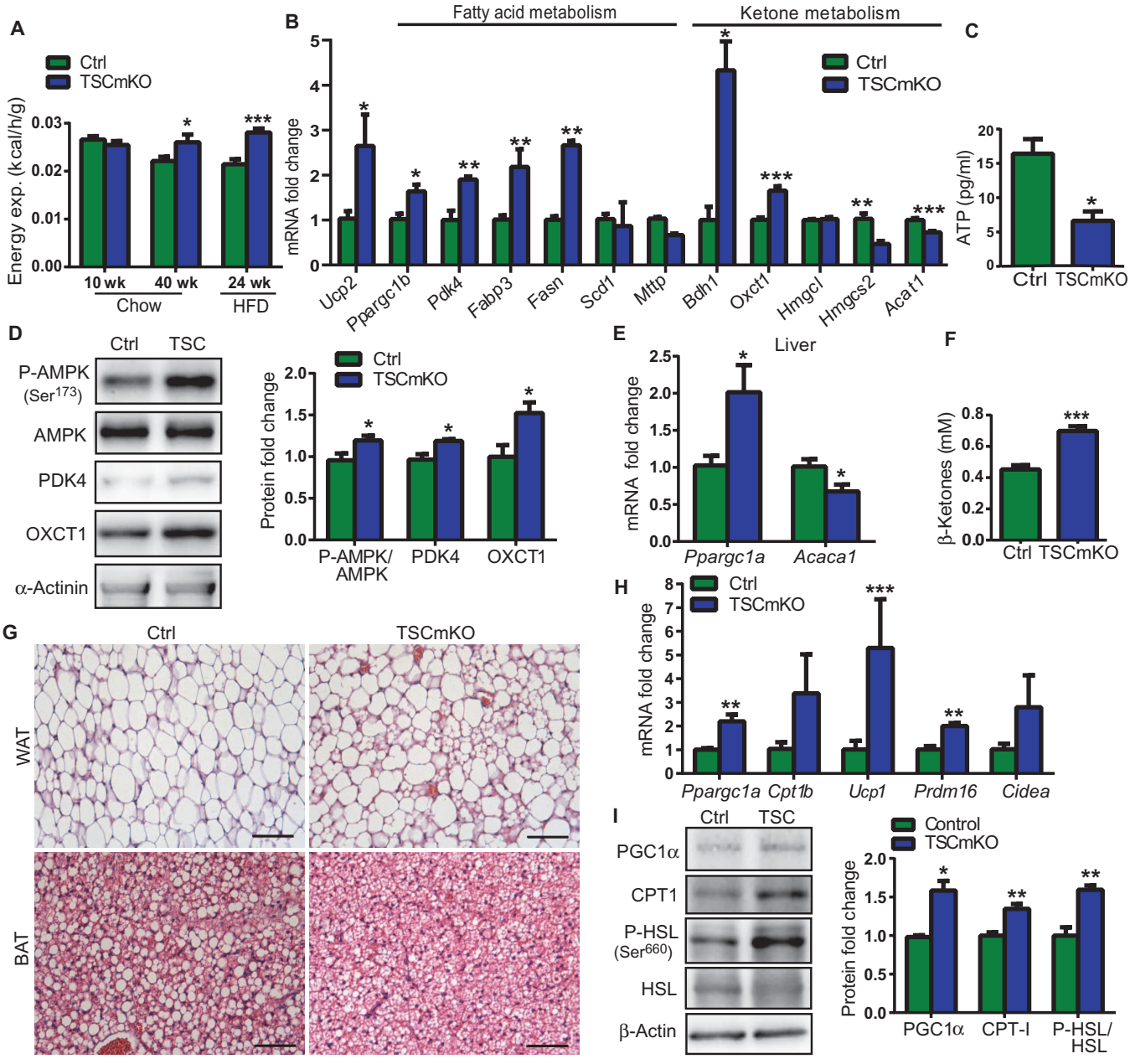

Fig. 2. TSCmKO mice show increased ketogenesis and fatty acid oxidation. (**A**) CLAMS (Comprehensive Lab Animal Monitoring System) analysis revealed normal energy expenditure in 10-week-old TSCmKO mice fed a chow diet ($n = 5$ mice per genotype), but a significant increase in 40-week-old mutant mice fed a chow diet ($n = 5$ mice per genotype) and in 24-week-old TSCmKO mice fed the HFD ($n = 6$ mice per genotype). (**B**) TSCmKO mice showed increased expression of genes involved in fatty acid oxidation (*Ucp2*, *Ppargc1b*, *Pdk4*, and *Fabp3*) and ketone catabolism (*Bdh1* and *Oxct1*) and reduced expression of ketogenesis genes (*Hmgcs2* and *Acat1*) in tibialis anterior (TA) muscle at 10 weeks of age ($n = 5$ mice per genotype). (**C**) TSCmKO mice showed decreased ATP concentrations in extensor digitorum longus (EDL) muscle at 10 weeks of age ($n = 5$ mice per genotype). (**D**) Immunoblots of TA muscle from 10-week-old TSCmKO (TSC) and control littermates are shown for the indicated phosphorylated (P-) and total proteins ($n = 8$ mice per genotype). Protein abundance was normalized to α-actinin. (**E**) Lower *Acac1* and higher *Ppargc1a* expression in the liver of 10-week-old TSCmKO mice ($n = 5$ mice per genotype). (**F**) Increased plasma β-ketone concentrations in 11-week-old TSCmKO mice revealed an increase in ketogenesis ($n = 10$ mice per genotype). (**G**) H&E staining of WAT and BAT from 12-week-old mice revealed increased browning of WAT and reduced lipid content in BAT of TSCmKO mice. Images are representative of four sections from three mice per genotype. Scale bars, 100 μm. (**H**) TSCmKO mice showed increased expression of genes involved in fatty acid oxidation (*Ppargc1a* and *Cpt1b*) and markers for browning (*Ucp1*, *Prdm16*, and *Cidea*) in inguinal-subcutaneous WAT at 12 weeks of age ($n = 5$ mice per genotype). (**I**) Immunoblots of WAT from 10-week-old TSCmKO and control littermates are shown for the indicated phosphorylated and total proteins ($n = 4$ mice per genotype). Protein abundance was normalized to β-actin. Data represent means ± SEM; $^{*}P < 0.05$, $^{**}P < 0.01$, $^{***}P < 0.001$.

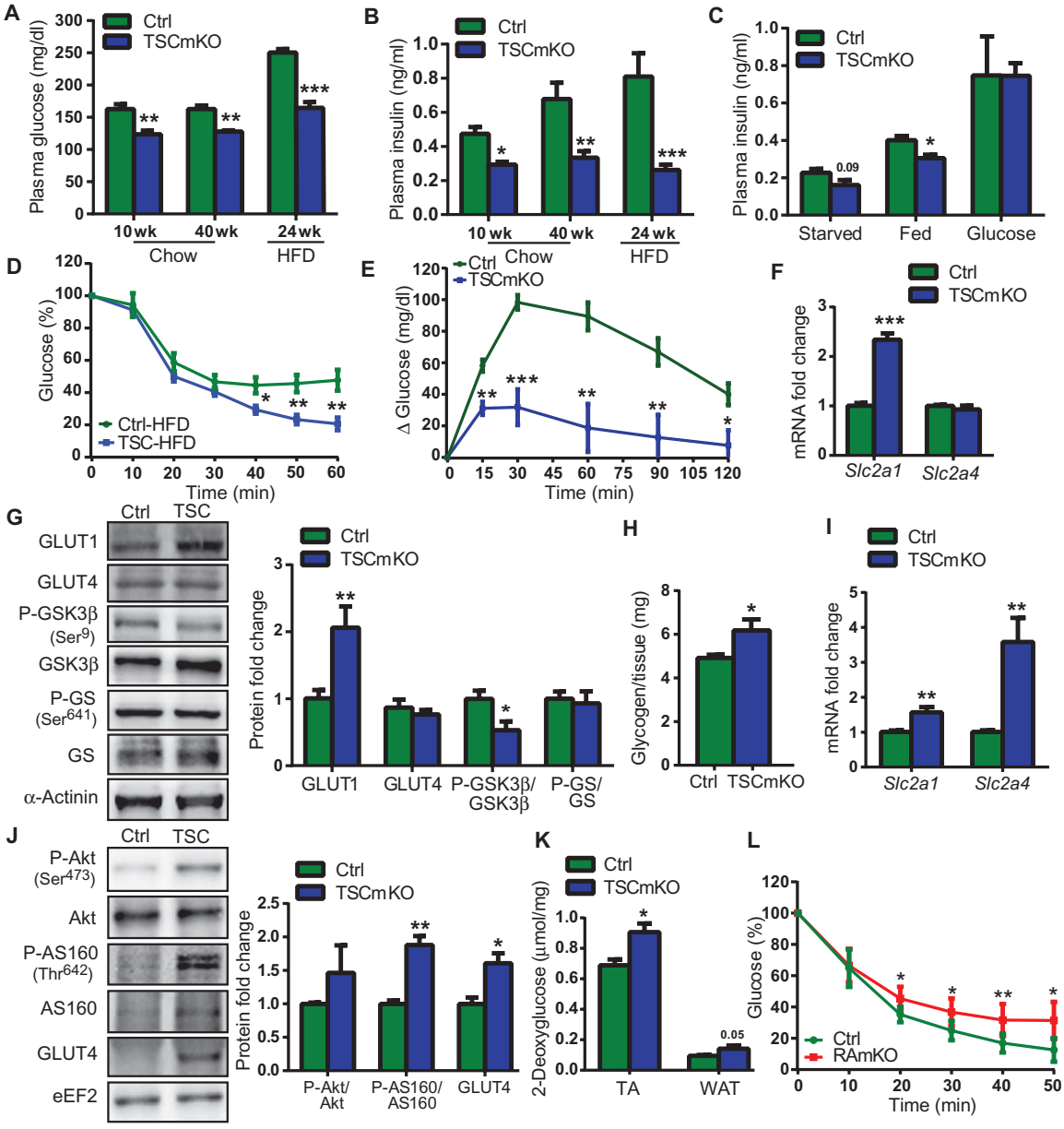

Fig. 3. TSCmKO mice show changes in glucose metabolism. (**A** and **B**) Decreased blood glucose (A) and plasma insulin (B) concentrations in 10- and 40-week-old TSCmKO mice fed a chow diet ($n = 8$ mice per genotype) and in 24-week-old mutant mice under the HFD ($n = 6$ mice per genotype). (**C**) Determination of plasma insulin concentration under starved or basal conditions and 20 min after glucose injection revealed normal glucose-stimulated insulin secretion in 10-week-old TSCmKO mice ($n = 5$ mice per genotype). (**D**) Insulin tolerance test performed on 24-week-old mice after 14 weeks of the HFD ($n = 6$ mice per genotype) revealed increased insulin sensitivity in TSCmKO mice. Linear regression analysis shows that the two groups differed significantly ($P = 0.01$). (**E**) Pyruvate tolerance test performed on 24-week-old mice revealed impaired liver gluconeogenesis in TSCmKO animals ($n = 4$ mice per genotype). Linear regression analysis shows that the two groups differed significantly ($P < 0.001$). (**F**) Ten-week-old TSCmKO mice showed increased expression of *Slc2a1* (which encodes GLUT1) and normal expression of *Slc2a4* (which encodes GLUT4) in TA muscle ($n = 4$ mice per genotype). (**G**) Immunoblots of TA muscle from 10-week-old TSCmKO and control mice are shown for the indicated phosphorylated and total proteins ($n = 4$ mice per genotype). Protein abundance was normalized to α-actinin. (**H**) Glycogen amount was increased in quadriceps muscle from 10-week-old TSCmKO mice ($n = 5$ mice per genotype). (**I**) TSCmKO mice showed increased expression of *Slc2a1* and *Slc2a4* (which encode GLUT1 and GLUT4) in inguinal-subcutaneous WAT at 12 weeks of age ($n = 6$ mice per genotype). (**J**) Immunoblots of WAT from 10-week-old TSCmKO and control mice are shown for the indicated phosphorylated and total proteins ($n = 4$ mice per genotype). Protein abundance was normalized to eukaryotic translation elongation factor 2 (eEF2). (**K**) Increased glucose absorption in the TA muscle and WAT of 10-week-old TSCmKO mice is shown by a higher accumulation of 2-deoxyglucose ($n = 3$ mice per genotype). (**L**) Insulin tolerance test performed on 10-week-old mice revealed insulin resistance in RAmKO mice ($n = 6$ mice per genotype). Linear regression analysis shows that the two groups differ significantly ($P = 0.04$). Data represent means ± SEM; $^*P < 0.05$, $^{**}P < 0.01$, $^{***}P < 0.001$.

conditions, rather than changes in glycolysis, might be responsible for the increase in glycogen in TSCmKO muscle.

The transcript and protein abundance of GLUT1 and GLUT4 were increased in the WAT of TSCmKO mice (Fig. 3, I and J), suggesting higher glucose uptake in this nonmuscle tissue. The phosphorylation (and activation) of Akt substrate of 160 kD (AS160) was also increased in the WAT of mutant mice (Fig. 3J); activated AS160 favors glucose absorption upon insulin signaling (*27*, *28*). An in vivo 2-deoxyglucose uptake test confirmed the increased glucose absorption in the muscle and WAT of mutant mice (Fig. 3K). In contrast, the expression of genes involved in glucose metabolism and transport was unchanged in the liver of TSCmKO mice (fig. S3D). These results indicated that sustained mTORC1 activity in skeletal muscle reduced glycemia because of the enhanced insulin sensitivity and increased glucose absorption in muscle and WAT.

To determine if these changes in glucose metabolism were a direct consequence of mTORC1 activity in muscle, we also examined glucose metabolism in RAmKO mice, which lack mTORC1 signaling in skeletal muscle (*17*). Although plasma glucose and insulin concentrations were unchanged in 10-week-old RAmKO mice (fig. S3, E and F), the mice were insulin-resistant when compared to control littermates (Fig. 3L). Together, these results point to a major role of mTORC1 signaling in muscle in regulating whole-body glucose metabolism.

TSCmKO muscle secretes FGF21

Changes in whole-body metabolism in the TSCmKO mice suggested the action of a secreted myokine (*3*). One candidate is FGF21, a starvation-induced hormone that can decrease glycemia and promote fatty acid oxidation (*5*). At the age of 10 weeks, plasma concentrations of FGF21 were not detectable by enzyme-linked immunosorbent assay (ELISA) in fed mice. As reported by others, 24-hour starvation increased FGF21 concentration (Fig. 4A). Plasma FGF21 concentrations were significantly higher in starved TSCmKO mice and were also higher in 24-week-old fed mutant

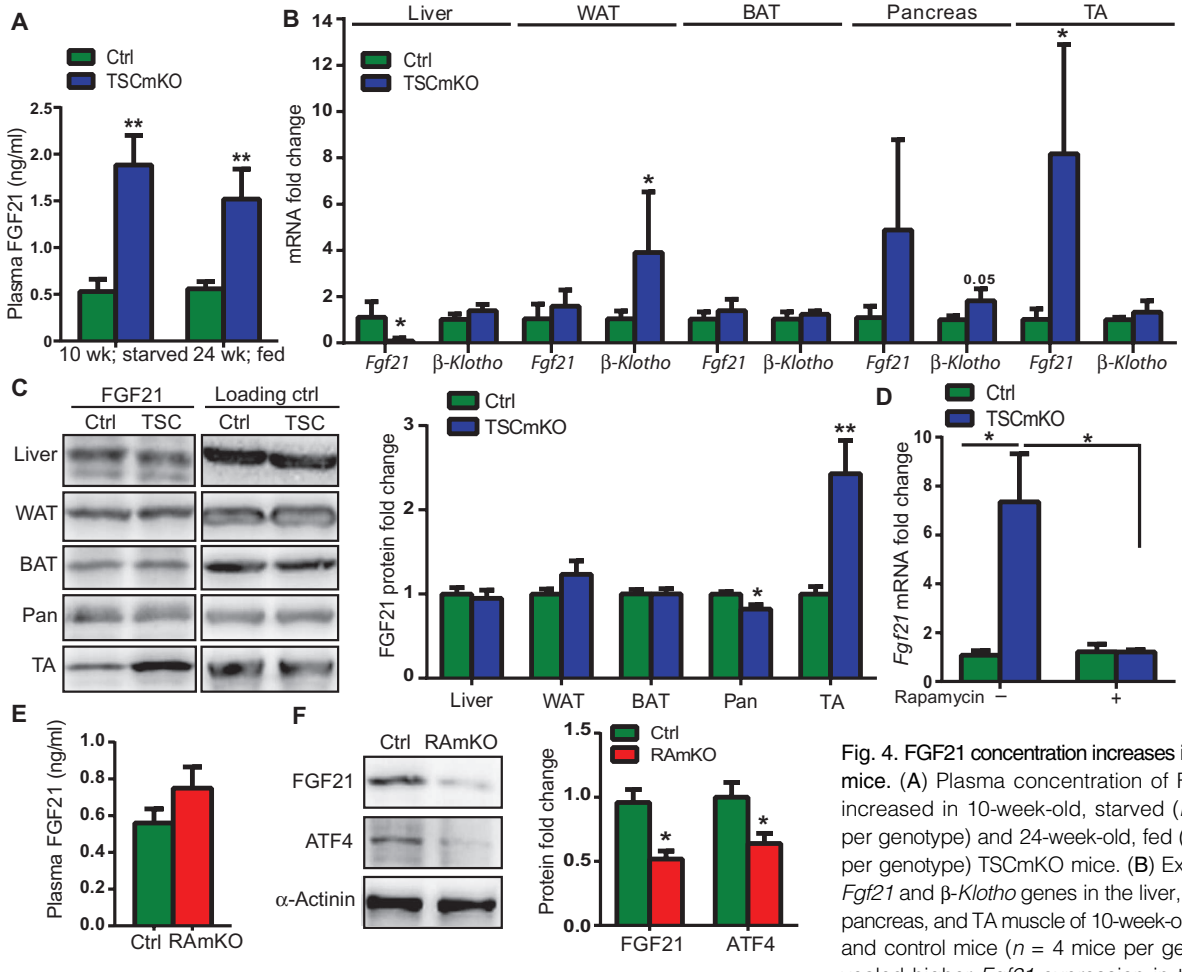

Fig. 4. FGF21 concentration increases in TSCmKO mice. (**A**) Plasma concentration of FGF21 was increased in 10-week-old, starved (n = 3 mice per genotype) and 24-week-old, fed (n = 6 mice per genotype) TSCmKO mice. (**B**) Expression of *Fgf21* and β-*Klotho* genes in the liver, WAT, BAT, pancreas, and TA muscle of 10-week-old TSCmKO and control mice (n = 4 mice per genotype) revealed higher *Fgf21* expression in the skeletal muscle of mutant mice. (**C**) Immunoblot analysis of FGF21 in the liver, WAT, BAT, pancreas (Pan), and TA muscle of 10-week-old TSCmKO and control mice (n = 4 mice per genotype). Protein abundance was normalized to β-actin for liver, WAT, and BAT; to eEF2 for pancreas; and to α-actinin for TA (loading control). (**D**) Increased *Fgf21* expression in the TA muscle of TSCmKO mice (n = 3 mice per genotype) was normalized after 3-day rapamycin treatment (n = 4 mice per genotype). (**E**) Plasma FGF21 concentration was not changed in 20-week-old RAmKO mice (n = 4 mice per genotype). (**F**) Immunoblot analysis of FGF21 and ATF4 is shown for the TA muscle of 10-week-old RAmKO mice (n = 4 mice per genotype). Protein abundance was normalized to α-actinin. Data represent means ± SEM; *P < 0.05,**P < 0.01.

mice compared to control littermates (Fig. 4A). These results were confirmed by Western blot analysis of plasma FGF21 (fig. S4A). Besides the liver, which is the main FGF21 secretory organ (*11*), FGF21 can also be secreted by WAT (*12*), BAT (*29*), pancreas (*30*), and skeletal muscle (*13*, *31*). Thus, to determine the origin of the increased plasma concentrations of FGF21 in mutant mice, we compared the transcript and protein abundance of FGF21 in these tissues between control and TSCmKO mice. Whereas *Fgf21* expression was significantly reduced in the liver of TSCmKO mice, it was significantly increased in the tibialis anterior (TA) muscle of mutant mice (Fig. 4B). β-*Klotho* encodes the essential co-receptor of FGF21 (*32*), and its expression was unaltered, except in WAT, where it was significantly increased (Fig. 4B). FGF21 protein abundance was unchanged in all organs but was increased in TSCmKO muscle (Fig. 4C). Moreover, HFD treatment increased the expression of *Fgf21* in the liver of control mice as previously reported (*11*), whereas *Fgf21* expression was unchanged in the liver of TSCmKO mice but significantly increased in the muscle of mutant mice (fig. S4B). This increase in FGF21 abundance was a direct consequence of mTORC1 signaling because 3-day treatment with the mTORC1 inhibitor rapamycin normalized *Fgf21* expression in TSCmKO muscle (Fig. 4D). Furthermore, whereas FGF21 plasma concentrations were unchanged in 20-week-old RAmKO mice (Fig. 4E), FGF21 protein abundance was significantly reduced in the targeted muscle (Fig. 4F). Together, these results indicate that the increased plasma FGF21 concentrations in TSCmKO mice originated from skeletal muscle, and they shed light on a role of mTORC1 signaling in regulating FGF21 in skeletal muscle.

mTORC1-activated ER stress induces FGF21 in skeletal muscle

Fgf21 expression in muscle correlates with increased abundance of ATF4 (*4*, *13*). ATF4 is a critical regulator of the integrated stress response, which is induced by various cellular stresses including amino acid depletion and ER or oxidative stress (*33*). In 10-week-old TSCmKO mice, the protein abundance of ATF4 was increased (Fig. 5A), whereas *Atf4* expression was not altered (fig. S5A). In contrast, the skeletal muscle of 12-week-old RAmKO mice contained lower amounts of ATF4 (Fig. 4F).

Two pathways have previously been implicated in the ATF4-mediated increase in FGF21 abundance in muscle: impaired autophagy and mitochondrial dysfunction (*4*, *13*). Autophagy induction is inhibited in the TSCmKO mice by phosphorylation of Unc-51 like autophagy activating kinase 1 (Ulk1) (*18*). Ulk1 is part of the autophagy initiation complex, and mutation of Ser^{757} in Ulk1 to Ala restores autophagy induction in TSCmKO mice (*18*). To examine the effect of autophagy on FGF21 abundance in TSCmKO muscle, we electroporated mutant Ulk1 into TA muscle. Despite partial restoration of autophagy in the electroporated muscle, we did not observe a decrease in FGF21 mRNA or protein abundance in TSCmKO mice (fig. S5, B and C). The electroporation per se did not affect FGF21 abundance (fig. S5, D and E). In contrast, autophagy restoration in control mice was sufficient to decrease FGF21 mRNA and protein abundance (fig. S5, B and C). TSCmKO mice at the age of 10 to 12 weeks did not show changes in mitochondrial DNA (*19*) or expression of genes involved in the mitochondrial respiratory chain or reactive oxygen species production (fig. S5F). Moreover, the oxidative capacity of TSCmKO muscle is enhanced (*19*), and the overall oxidation status of muscle proteins was not changed in mutant muscle (fig. S5G). These results indicated the existence of another pathway that mediated the increase in ATF4 and FGF21 abundance in the TSCmKO mice.

Indeed, examination of TSCmKO muscle by electron microscopy revealed the presence of irregularly shaped ER clusters (Fig. 5B) suggestive of dysfunctional ER and ER stress (*34*). The ER stress pathway that leads to an increase in ATF4 abundance acts through PERK, which in turn inhibits its downstream target, eIF2α (*35*). Indeed, like ATF4 abundance, the phosphorylation of PERK and eIF2α was increased in TSCmKO muscle (Fig. 5A). In addition, the abundance of the ER stress marker binding immunoglobulin protein (BiP) was significantly increased (Fig. 5A). Upon activation of ER stress, the unfolded protein response (UPR) is initiated to reestablish normal ER function (*35*). TSCmKO muscle had increased expression of genes involved in the UPR—such as *DNA damage–inducible transcript 3* (*Ddit3*), which encodes CHOP, a proapoptotic transcription factor; *heat shock 70 kD protein 5* (*Hspa5*), which encodes the ER chaperone BiP; *X-box binding protein 1* (*Xbp1*), which encodes a transcription factor that controls genes involved in protein folding; and *Tribbles homolog 3* (*Trib3*), which is induced by CHOP and is involved in cell death (*36*, *37*) (Fig. 5C). Increased mTORC1 activity has been proposed to induce ER stress by increasing protein translation (*38*). Accordingly, protein synthesis (*19*) and protein translation (fig. S5H) were increased in TSCmKO muscle. Moreover, rapamycin treatment significantly decreased the expression of *Hspa5* and *Ddit3* in TSCmKO and control mice (fig. S5I), demonstrating a role for mTORC1 in ER stress induction. To confirm that changes in mTORC1 signaling can directly modulate FGF21 abundance in muscle fibers, we studied the regulation of FGF21 in vitro. Acute mTORC1 activation in C2C12 myotubes by insulin induced FGF21 at the mRNA and protein levels, an effect that was abolished by pretreatment of the cells with rapamycin (Fig. 5, D and E). Similarly, the ER stress inducer thapsigargin also promoted the accumulation of FGF21 at the mRNA and protein levels (Fig. 5, D and E). These results provide independent evidence suggesting that mTORC1 activation and ER stress induce FGF21 in muscle cells.

Finally, to test directly whether alleviation of ER stress would normalize FGF21 in vivo, we treated control and TSCmKO mice with 4-phenylbutyric acid (4-PBA), a chemical chaperone that assists in protein folding (*39*). Four-week treatment decreased the abundance of ATF4 and the phosphorylation of PERK and eIF2α (Fig. 5F). Moreover, expression of the ER stress markers *Ddit3*, *Hspa5*, *Xbp1*, and *Trib3* was reduced in TSCmKO muscle treated with 4-PBA (Fig. 5G). In addition, the treatment and ER stress alleviation also decreased FGF21 mRNA expression and protein abundance (Fig. 5, F and G). Together, these results suggest that ER stress caused by sustained mTORC1 activation is the main cause for the induction of FGF21 in TSCmKO muscle.

Blocking of FGF21 normalizes the metabolism of TSCmKO mice

Because 4-PBA treatment decreased FGF21 abundance in the muscle of TSCmKO mice, we also tested whether this treatment would normalize the metabolism of these mice. The 4-week treatment prompted a significant, progressive weight gain in TSCmKO mice (Fig. 6A) that was likely due to an increase in lean mass (Fig. 6B). Body temperature, which is decreased in FGF21 transgenic mice (*7*) and was significantly lower in TSCmKO mice (Fig. 6C), was also normalized by 4-PBA treatment (Fig. 6C). Blood glucose concentrations were the same in control and mutant mice after the treatment (fig. S6A), whereas insulin concentration remained low (fig. S6B).

To directly test whether blocking FGF21 would affect metabolism, we next injected an FGF21-neutralizing antibody (*40*) into 12- and 24-week-old TSCmKO mice. As expected, plasma concentrations of FGF21 were significantly decreased after FGF21 antibody administration (fig. S6C). Injection of the antibody also normalized blood β-ketone (Fig. 6D) and blood glucose concentrations (Fig. 6E). Similar to the 4-PBA treatment, plasma insulin concentrations were not affected (fig. S6D). Inhibition of plasma FGF21 also improved liver gluconeogenesis in 24-week-old TSCmKO mice, as reflected by an increase in the rate of glucose production

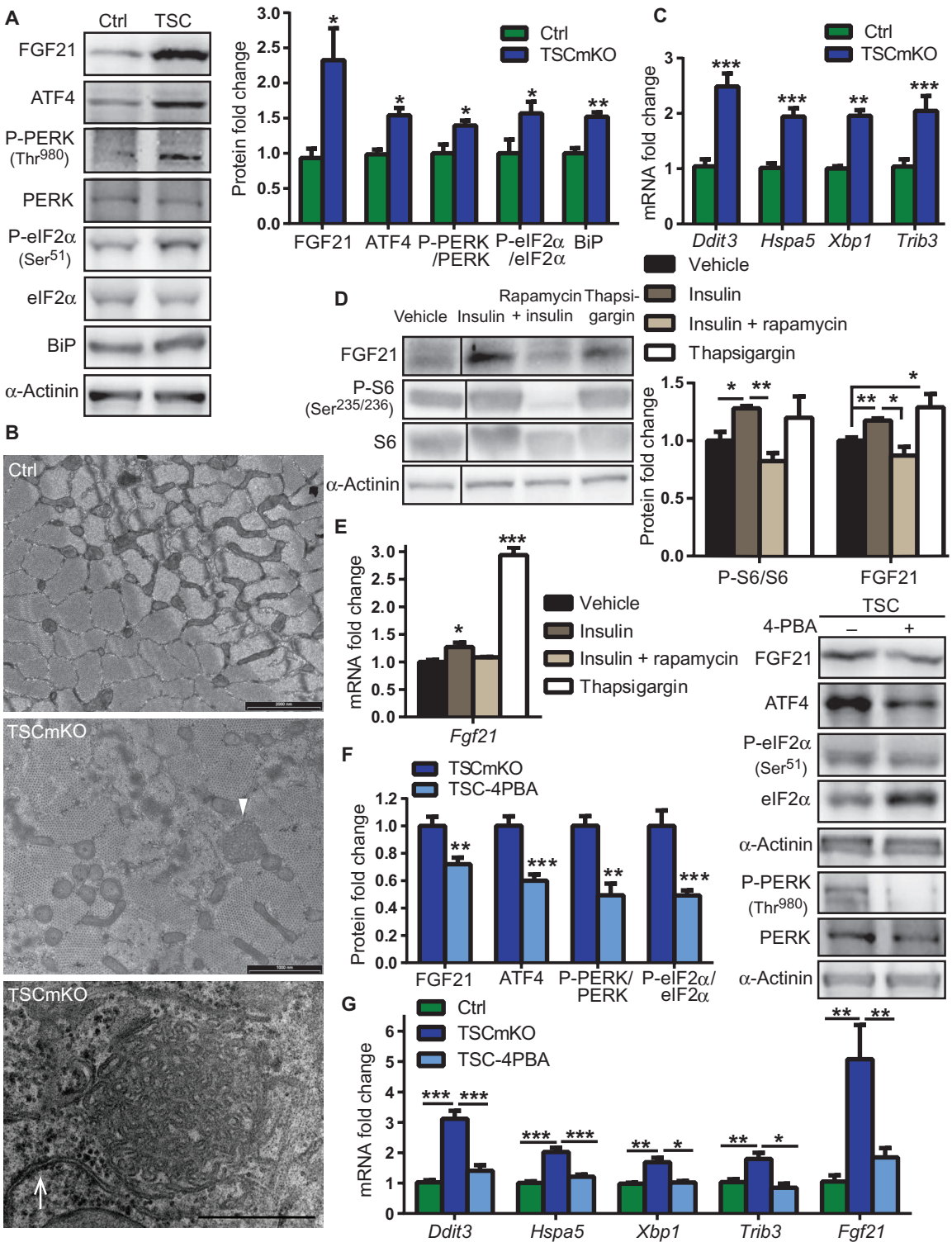

Fig. 5. Activation of mTORC1 increases FGF21 abundance in skeletal muscle through ER stress–mediated induction of the PERK-eIF2α-ATF4 pathway. (**A**) Immunoblots of TA muscle from 10-week-old TSCmKO and control mice are shown for the indicated phosphorylated and total proteins (n = 5 mice per genotype), which indicated an activation of ER stress. Protein abundance was normalized to α-actinin. (**B**) Electron microscopic images of EDL muscle from 40-week-old control and TSCmKO mice revealed ER aggregates in mutant muscle. Arrowhead and arrow point to ER cluster and rough ER detail, respectively. Scale bars, 2000 nm (top); 1000 nm (middle); 500 nm (bottom). Images are representative of three mice per genotype. (**C**) TSCmKO mice showed increased expression of ER stress and UPR markers in TA muscle at 10 weeks of age (n = 5 mice per genotype). (**D**) Immunoblots from C2C12 myotubes treated with insulin and thapsigargin showed accumulation of FGF21 upon mTORC1 activation and ER stress induction, which was abolished with rapamycin treatment (n = 4 sets of cells per condition). Protein abundance was normalized to α-actinin. (**E**) C2C12 myotubes treated with insulin and thapsigargin showed increased transcriptional expression of *Fgf21*, which was blunted by rapamycin treatment (n = 4 sets of cells per condition). (**F**) Immunoblots of TA muscle are shown for the indicated phosphorylated and total proteins in 4-PBA–treated TSCmKO mice (+) compared to untreated (–) mice (n = 7 mice per genotype and treatment). Protein abundance was normalized to α-actinin. (**G**) 4-PBA treatment normalized the expression of UPR markers and *Fgf21* in gastrocnemius and TA muscle from 14-week-old TSCmKO mice (n = 7 mice per genotype and treatment). Data represent means ± SEM; $^{*}P < 0.05$, $^{**}P < 0.01$, $^{***}P < 0.001$.

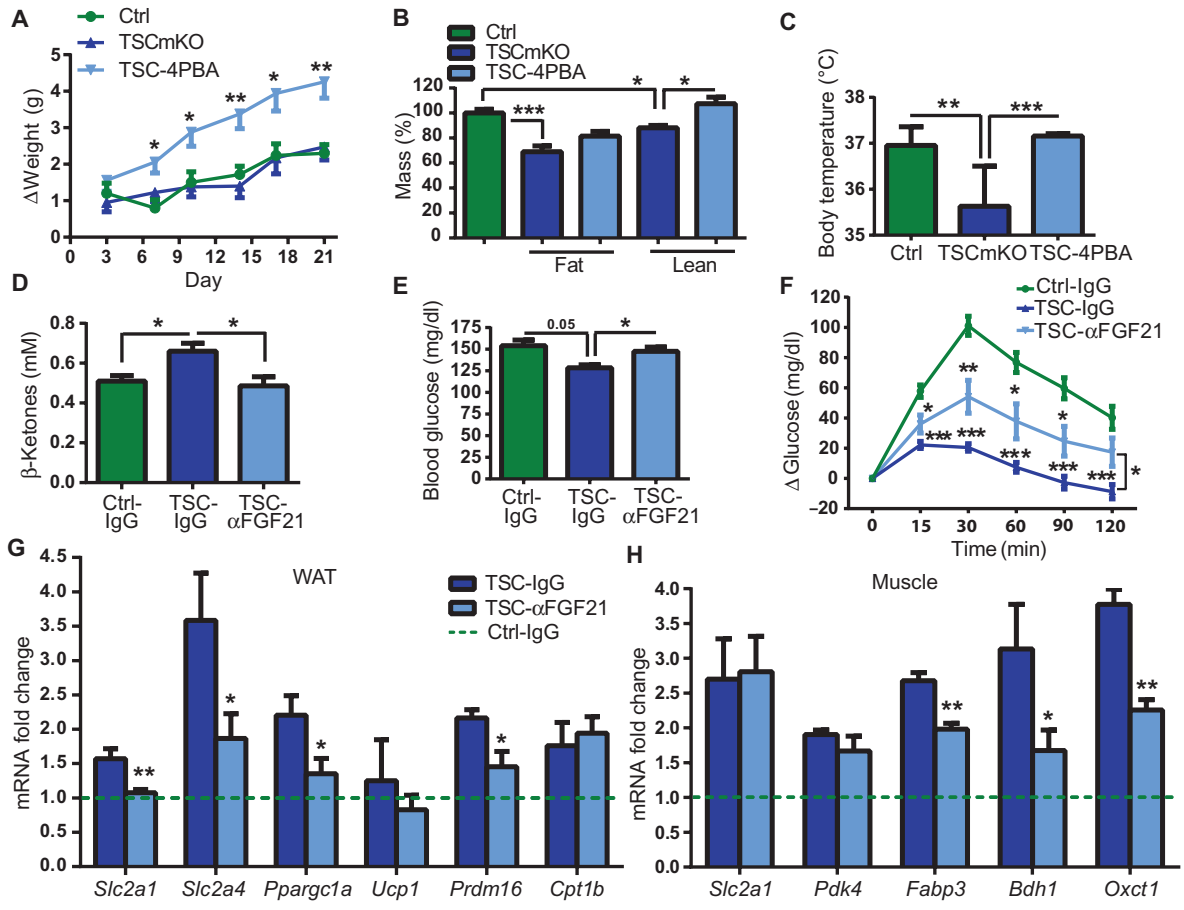

Fig. 6. Blocking FGF21 normalizes liver gluconeogenesis and plasma β-ketone and glucose concentrations. (**A**) Body weight of TSCmKO mice significantly increased after 3 weeks of 4-PBA treatment (n = 5 mice per genotype and treatment). Linear regression analysis shows that the groups differed significantly (P = 0.01). (**B**) Echo-MRI analysis of body composition showed changes in fat and lean mass percentage in TSCmKO mice after 4 weeks of 4-PBA treatment (n = 5 mice per genotype and treatment). (**C**) Body temperature was decreased in 14-week-old TSCmKO mice, but normalized after 4 weeks of 4-PBA treatment (n = 7 mice per genotype and treatment). (**D** and **E**) Blood β-ketone (D) and glucose (E) concentrations were normalized in 11-week-old TSCmKO mice treated with FGF21-neutralizing antibody (n = 13), compared to mutant (n = 5) and control (n = 13) mice treated with rabbit IgG. (**F**) After treatment with FGF21-neutralizing antibody, gluconeogenesis was improved in TSCmKO mice (n = 6) when compared to mutant (n = 3) and control (n = 9) mice treated with rabbit IgG. Linear regression analysis shows that the groups differed significantly (P < 0.001). (**G**) Expression of genes encoding glucose transporters (*Slc2a1* and *Slc2a4*), enzymes involved in fatty acid oxidation (*Ppargc1a* and *Cpt1b*), and browning markers (*Ucp1* and *Prdm16*) in WAT was normalized to varying extents after FGF21-neutralizing antibody treatment in 11-week-old TSCmKO mice (n = 7) when compared to TSCmKO (n = 5) and control mice treated with rabbit IgG (n = 8). Control line (Ctrl-IgG) represents the normalized gene expression of the IgG-treated littermates. (**H**) Expression of genes encoding proteins involved in fatty acid and ketone body breakdown (*Fabp3*, *Bdh1*, and *Oxct1*) in TA muscle was decreased after FGF21-neutralizing antibody treatment in 11-week-old TSCmKO mice (n = 7) when compared to TSCmKO (n = 5) and control mice (n = 8) treated with rabbit IgG. Control line (Ctrl-IgG) represents the normalized gene expression of the IgG-treated littermates. Data represent means ± SEM; *P < 0.05, **P < 0.01, ***P < 0.001.

when compared to immunoglobulin G (IgG)–injected TSCmKO mice (Fig. 6F). On the contrary, treatment of control mice with the FGF21-neutralizing antibody did not change plasma glucose, insulin, and ketone body concentrations or pyruvate tolerance (fig. S6, F and I). Finally, FGF21 neutralization significantly reduced the expression of *Slc2a1*, *Slc2a4*, *Ppargc1a* (*41*), and *Prdm16* in the WAT of TSCmKO mice without changing that of *Ucp1* and *Cpt1b* (Fig. 6G). These results are consistent with FGF21 promoting glucose absorption and fatty acid oxidation in the WAT of TSCmKO mice through transcriptional regulation. In addition, FGF21 neutralization decreased the expression of *Fabp3*, *Bdh1*, and *Oxct1* in skeletal muscle without changing that of *Slc2a1* and *Pdk4* (Fig. 6H), which correlates with a decrease in fatty acid oxidation and ketone body utilization. Control mice treated with the FGF21-neutralizing antibody showed increased expression of *Slc2a1*, *Slc2a4*, and *Fgf21* in WAT, with no changes in gene expression in muscle or liver (fig. S6J). In contrast, overnight treatment with the FGF21 antibody was not sufficient to normalize the expression of *Ppargc1a* in the liver of TSCmKO mice (fig. S6E). Together, these results suggest that FGF21 secreted by TSCmKO muscle is responsible for the overall metabolic changes in these mice and that it acts directly on non-muscle tissues, such as WAT, to modify glucose and fatty acid metabolism.

DISCUSSION

Skeletal muscle represents roughly 40% of the whole-body mass and thereby is the major supplier of amino acids for other metabolic organs like liver, in addition to being involved in the maintenance of metabolic homeostasis. We have previously shown that sustained mTORC1 activation in skeletal muscle blocks autophagy induction and causes a late-onset myopathy (*18*). Here, we described how the metabolic phenotype of TSCmKO mice changed with age. We then characterized the underlying molecular pathways in young, healthy mice to ensure that metabolic changes were not secondary to the late-onset myopathy (*18*). TSCmKO mice were lean, which correlated with improved insulin sensitivity and increased fatty acid oxidation. The leanness was likely caused by mTORC1 inducing FGF21 as a myokine through the ER stress–induced activation of ATF4. Consistent with this interpretation, attenuation of ER stress by 4-PBA decreased FGF21 mRNA and protein abundance and alleviated several of the disease symptoms in TSCmKO mice. In addition, direct inhibition of circulating FGF21 with a neutralizing antibody also normalized most of the TSCmKO metabolic phenotype. Thus, in TSCmKO mice, the mTORC1 pathway in skeletal muscle regulates body-wide energy metabolism through FGF21.

Perturbations of mTORC1 in other tissues, such as WAT or liver, can affect leanness in mice (*15*, *42*, *43*). Surprisingly, both activation and inhibition of mTORC1 result in resistance to diet-induced obesity, although specific consequences in other, nontargeted metabolic organs and the potential contribution of circulating factors have not been investigated and leanness has been attributed to different molecular mechanisms in the targeted tissues. Here, we also identified molecular changes in the targeted muscle tissue that might contribute to the metabolic phenotype of TSCmKO mice, such as modifications in *Ucp2*, *Ppargcb*, and GLUT1 mRNA and protein abundance. In addition, we identified mTORC1-triggered ER stress in skeletal muscle as the main driver of the metabolic changes observed on the whole-body level. We have previously reported that overall protein synthesis in TSCmKO muscle is increased (*19*), and here we showed an increase in translation initiation. Uncontrolled protein synthesis can result in ER stress and activate the UPR by overwhelming the folding capacity of the ER (*38*, *44*). In an initial physiological response, induction of UPR effectors, such as PERK, leads to a global translational attenuation through inhibition of eIF2α and to the activation of chaperones to relieve the ER stress. In contrast, unresolved ER stress and chronic activation of the UPR promote apoptosis by the activation of ATF4 downstream targets, such as CHOP and GADD34 (*35*). In TSCmKO muscle, the PERK-eIF2α-ATF4 pathway was activated, and chaperones and ER stress markers were increased. Decreased Akt activity in TSCmKO muscle (*19*) may also contribute to the increased activity of PERK and the activation of the eIF2α-ATF4 pathway because PERK is inhibited by Akt-dependent phosphorylation (*45*). Furthermore, consistent with the previously described ER conformational changes upon ER stress (*34*, *46*), muscle fibers of TSCmKO mice contained swollen tubules and aggregated clusters. We conclude that ER stress in the muscle of TSCmKO mice is driven by the increase in protein synthesis and translation initiation caused by activated mTORC1.

We found that ER stress induced changes in whole-body metabolism through activation of ATF4, which in turn induces FGF21 (*4*). We described the broad metabolic effects of FGF21 as a myokine, including changes in energy expenditure, ketogenesis, gluconeogenesis, fat mass, body temperature, and growth. These metabolic perturbations were consistent with the phenotype of FGF21-overexpressing transgenic mice (*7*, *8*), and some of these effects have been attributed to FGF21 secreted from skeletal muscle (*4*, *13*). Although these studies have linked increased FGF21 abundance in skeletal muscle to disturbances of mitochondrial integrity or autophagy impairment, we did not observe changes in the expression of mitochondrial genes or oxidative stress in the skeletal muscle of young TSCmKO mice. In addition, partial restoration of autophagy did not normalize FGF21 abundance in TSCmKO muscle. The induction of FGF21 in skeletal muscle has been linked to activation of the phosphatidylinositol 3-kinase (PI3K)–Akt pathway (*31*), which we showed was due to mTORC1 activation and its effect on ER stress, because Akt activity was attenuated in TSCmKO muscle, presumably due to the negative feedback loop of S6 kinase (S6K) on insulin receptor substrate 1 (IRS-1), which in turn dampened PI3K-Akt signaling (*19*). In support of this notion, activated mTORC1 in liver-specific TSC1 knockout mice also leads to FGF21 secretion (*47*), and both ATF4 and FGF21 abundance were reduced in RAmKO muscle.

We showed that the main molecular mechanism driving FGF21 synthesis relied on mTORC1-induced ER stress. Increased mTORC1 activity or ER stress induced the accumulation of FGF21 in C2C12 myotubes. We further confirmed this molecular pathway by treating TSCmKO mice with 4-PBA, a Food and Drug Administration–approved chemical chaperone that is a candidate drug to treat diabetes, cancer, and protein misfolding diseases (*39*, *48*). In TSCmKO muscle, 4-PBA treatment attenuated ER stress by reducing PERK-eIF2α-ATF4 signaling, decreased the expression of UPR markers, and reduced FGF21 mRNA and protein abundance without affecting mTORC1 activity. Long-term treatment with 4-PBA also increased the weight of the TSCmKO mice and normalized their body temperature.

The metabolic phenotype of TSCmKO mice is reminiscent of the action of FGF21 on metabolic organs. WAT is the main target tissue of FGF21 (*8*, *32*, *49*), and TSCmKO WAT showed increased mRNA and protein abundance of many regulators of browning, fatty acid oxidation, and glucose metabolism, which were associated with increased glucose uptake and lipolysis. In addition, WAT was the only tissue in TSCmKO mice that showed significantly increased expression the gene encoding the β-Klotho receptor, an effect that is also seen in mice with increased plasma FGF21 concentration (*13*) or in cultured adipocytes treated with FGF21 (*50*). The liver of TSCmKO mice showed increased expression of *Ppargc1a*, which correlates with increased fatty acid oxidation induced by FGF21 (*11*, *51*). FGF21 also induces ketogenesis in the liver (*7*) and TSCmKO mice had higher plasma β-ketone concentration and increased expression of genes involved in ketone body breakdown in muscle. TSCmKO mice also had reduced liver gluconeogenesis, which is consistent with the suppression of hepatic gluconeogenesis by FGF21 (*52*, *53*).

We showed that acute inhibition of FGF21 in the blood with an FGF21-blocking antibody normalized several of the metabolic traits of TSCmKO mice, such as plasma β-ketone and glucose concentrations, thus confirming the functional role of FGF21 as a hormone in the mutant mice. The decreased plasma concentration of β-ketones was associated with reduced expression of genes involved in ketone body breakdown in skeletal muscle. Similarly, normalization of plasma glucose concentration after blocking of FGF21 could be the result of improved liver gluconeogenesis and lower glucose uptake by WAT, which could be due to normalized expression of glucose transporter–encoding genes. Likewise, markers of fatty acid oxidation and browning were also normalized in WAT. In skeletal muscle, however, the increased expression of several metabolic genes in TSCmKO mice was not affected by inhibition of plasma FGF21, suggesting that those genes were induced by the autocrine action of FGF21 or directly by mTORC1 activation.

The phenotype of TSCmKO mice resembles the metabolism characteristic of starvation in several aspects. The "starvation" signal in TSCmKO mice could reflect the mTORC1-dependent increase in anabolic processes, which results in substantial energy depletion and exhaustion of ATP stores, as has been described in other TSC-deficient cell types (*54*, *55*). As in starvation, where liver is the main source for the increase in plasma FGF21 concentrations (*56*), the increase of FGF21 in the plasma of TSCmKO mice could constitute a stress signal to other metabolic organs to deliver

fatty acids to muscle and might be the cause of the progressive loss of fat mass. Constitutive mTORC1 activity also renders hypoxic cells critically dependent on exogenous unsaturated lipids for survival because of the induction of the UPR by deregulated lipid and protein synthesis in tumor cells (*55*). In addition, many highly aggressive human cancers trigger increased release of fatty acids from lipid stores, contributing to the cachexia observed in patients. Furthermore, plasma FGF21 concentration is increased in HIV patients, and increased skeletal muscle FGF21 abundance has been specifically linked with lipodystrophy and lipid disturbances in these patients (*57*, *58*). Although FGF21-overexpressing transgenic mice are lighter and resistant to obesity, they do not develop lipodystrophy (*8*, *59*), which suggests that stress-induced FGF21 could have disease-specific effects. In this context, solving the mechanisms of mTORC1-induced FGF21 secretion adds valuable knowledge in understanding disease-related metabolic changes that occur in pathologies, such as diabetes, cancer, or HIV.

In addition to its positive effects on obesity and diabetes (*6*), FGF21 can have detrimental consequences, including growth retardation (*60*, *61*), lower body temperature, and decreased activity (*7*). Moreover, FGF21 decreases female fertility (*62*) and causes bone loss (*50*). Some of these aspects, such as lower body temperature and impaired growth, were also observed in the TSCmKO mice. The body temperature in the TSCmKO mice was reduced upon fasting, which is likely a direct effect of FGF21 causing torpor to conserve energy (*7*, *47*). On the other hand, impaired growth in TSCmKO mice might be a consequence of decreased IGF-1 plasma concentration due to FGF21 action in the liver, as observed in other mouse models with increased plasma FGF21 (*7*, *13*). Because changes in mTORC1 activity cause the perturbations observed in TSCmKO mice, it would also be interesting to investigate FGF21 signaling in other muscle pathologies in which mTORC1 signaling is deregulated (*63*, *64*). Nevertheless, our results suggest that alterations in mTORC1 signaling in skeletal muscle can directly affect whole-body metabolism, and they define the broad effects of muscle-secreted FGF21. Moreover, our study may bring new insights into the mechanisms responsible for metabolic changes that arise from altered muscle integrity and health.

MATERIALS AND METHODS

Mice

Generation of TSCmKO and RAmKO transgenic mice and their genotyping have been previously described (*17*, *18*, *65*). Control mice were littermates floxed for *Rptor* (gene encoding raptor) or *Tsc1* but not expressing Cre-recombinase. Mice were maintained in a conventional facility with a fixed light cycle (23°C, 12-hour dark-light cycle) and were fed standard chow (KLIVA NAFAG, 1304811) or an HFD containing 60% fat (KLIBA NAFAG, 2127.PH.A05) ad libitum. HFD was started at 10 weeks of age and continued for 14 weeks. CLAMS and HFD analysis were performed only in male mice, whereas other experiments were performed both in male and female mice. In some experiments, mice were intraperitoneally injected with rapamycin (LC Laboratories, 2 mg/kg) for 3 days, as described previously (*66*). Euthanasia was performed at 10 a.m. after food removal at 6 a.m. the same morning, except for the FGF21-neutralizing antibody–injected mice, which were euthanized at 2 p.m., with food removal at 9 a.m. All procedures were performed in accordance with Swiss regulations for animal experimentation and approved by the veterinary commission of the Canton Basel-Stadt.

Body composition analysis

Magnetic resonance analysis of body composition (fat, lean, and water measurements) was performed in conscious immobilized mice, using the EchoMRI-100H body composition analyzer (EchoMRI).

Animal monitoring

Analysis of global metabolic parameters and behavior of mice was performed by the use of CLAMS. Mice were individually caged and adapted to their new environment for 1 day before starting the measurements, which were done for the following 3 or 4 days. Food and water intake, oxygen consumption, CO_2 consumption, heat, and activity were determined with Oxymax software (Columbus Instruments).

Blood analyses

Blood was obtained from the tail veins of living mice. For glucose measurement, food was removed at 9 a.m. and glucose was measured at 2 p.m. with the One Touch Ultra Easy glucose meter (LifeScan Inc.). Plasma β-ketone and FGF21 measurements were performed at 9 a.m. in the morning in mice fed ad libitum, using the Freestyle Precision β-ketone meter (Abbott Diabetes Care Ltd.) and the Mouse and Rat FGF-21 ELISA kit (BioVendor), respectively. FGF21 and free fatty acid analysis in starved mice was conducted at 9 a.m., with food deprivation at 6 p.m. Plasma free fatty acid concentrations were measured using the HR Series NEFA-HR kit (Wako). Plasma IGF-1, GH, and insulin concentrations were measured at 9 a.m. in the morning, after food removal at 6 a.m., using the Mouse/Rat IGF-I Quantikine ELISA kit (R&D Systems), Mouse Growth Hormone ELISA kit (Crystal Chem Inc.), and Ultra-Sensitive Mouse Insulin ELISA kit (Crystal Chem Inc.), respectively. Triglyceride and cholesterol concentrations were measured with a Cobas C111 machine (Roche), from the same plasma obtained at 9 a.m. after food removal at 6 a.m.

Glucose, insulin, and pyruvate tolerance tests

Glucose and pyruvate tolerance tests were performed in overnight (16-hour) fasted mice by intraperitoneal injection of glucose (1.5 g/kg; Merck) and pyruvate (Sigma-Aldrich), respectively. Insulin tolerance test was performed in 5-hour fasted mice at 2 p.m., after intraperitoneal injection of insulin (0.75 U/kg; Humalog, Eli Lilly). The guidelines from the Vanderbilt Mouse Metabolic Phenotyping Center (MMPC) program were followed for glucose homeostasis experiments (*67*).

4-PBA treatment

Mice were treated with 4-PBA (Sigma) at 1 g/kg per day, starting at the age of 10 weeks. 4-PBA was diluted in drinking water at 10 mg/ml, pH was adjusted to 7.34, and the solution was filtered through a 0.22-μm filter and kept at 4°C. Mice were given free access to the drinking solution, which was changed every 3 days, and the remaining volume was measured to calculate the intake of each mouse. Mice were weighed every 3 days during the 4 weeks of the treatment.

FGF21-neutralizing antibody

Mice were intraperitoneally injected with an FGF21-neutralizing monoclonal antibody (250 μg/kg; AIS, The University of Hong Kong) diluted in 0.9% NaCl solution at 6 p.m. Control groups were intraperitoneally injected with purified rabbit IgG (250 μg/kg; ChromPure Rabbit IgG, Jackson ImmunoResearch Laboratories Inc.) diluted in 0.9% NaCl (*40*, *68*).

Body temperature measurement

Body temperature was measured using an rectal thermometer (Physitemp BAT-12, Physitemp Instruments Inc.) at 5 p.m. in 8-hour fasted conscious mice.

Muscle ATP measurement

To determine ATP content in skeletal muscle, a luminescence assay was used (CellTiter-Glo Luminescent Cell Viability Assay, Promega). Frozen EDL muscle was homogenized in 0.2 ml of lysis buffer (0.2% Triton X-100, 4 mM

EDTA in water), and the homogenate was cleared by centrifugation at 14,000 rpm, 4°C, 15 min. The supernatant was diluted in phosphate-buffered saline (PBS), and the reaction mix, containing luciferase and substrate, was added. Luminosity was measured using a Tecan Infinite F500 luminometer (Tecan) and quantified according to an ATP standard curve (Sigma-Aldrich).

Muscle glycogen measurement

For the analysis of muscle glycogen content, a glycogen assay kit was used (Sigma-Aldrich). Frozen quadriceps muscle was homogenized, one half in 2 M HCl solution and the other half in 2 M NaOH solution. Samples were boiled at 95°C for 1 hour and centrifuged at 14,000 rpm for 10 min, and the supernatant was then mixed with glucose and the assay reagent as determined by the manufacturer. Glycogen was determined by absorbance using a spectrophotometer (Ultrospec II, LKB Biochrom).

In vivo 2-deoxyglucose uptake measurement

To measure glucose uptake into TA muscle and WAT, a 2-deoxyglucose uptake measurement kit was used (Cosmo Bio Co.). After food removal at 9 a.m., mice were intraperitoneally injected with insulin at 0.75 U/kg (Humalog, Eli Lilly). Ten minutes later, mice were intraperitoneally injected with 5 μg of 2-deoxyglucose (Sigma). Mice were sacrificed 45 min after 2-deoxyglucose injection, and tissues were dissected for further analysis. WAT (50 mg) and TA muscle (10 mg) were homogenized in 500 μl of 10 mM tris-HCl (pH 8.1) and then incubated at 95°C for 15 min. Samples were centrifuged for 15 min at 17,800*g* (4°C), and the supernatant was diluted in 10 mM tris-HCl (*69*). Diluted samples (20 μl) were used for further analysis according to the manufacturer's instructions (Cosmo Bio Co.) for a final absorbance measurement according to a 2-deoxy-D-glucose-6-phosphate standard curve.

In vivo muscle electroporation

Electroporation into muscle fibers and Ulk1 plasmid generation were performed as previously described (*18*, *70*).

Cell culture

Mouse C2C12 myoblasts were maintained at 37°C and 5% CO_2 in Dulbecco's modified Eagle's medium (DMEM) containing antibiotics [penicillin (100 U/ml), streptomycin sulfate (100 μg/ml)], L-glutamine, sodium pyruvate, and 20% fetal bovine serum (FBS). Myoblasts were set up for experiments on day 0 in six-well plates at a density of 7500 cells/cm^2. On day 2, differentiation was induced by replacing 20% FBS with 2% FBS, and the medium was changed every 2 days afterward. On day 6, cells were treated with DMEM containing 10 nM insulin (Sigma) or 500 nM thapsigargin (Tocris Bioscience). For the inhibition group, cells were pretreated with 100 nM rapamycin (LC Laboratories) for 15 min before the addition of insulin. For the control group, cells were treated with the vehicle, containing dimethyl sulfoxide and ethanol in DMEM. One hour after treatment, wells were washed once with warm PBS, and cells were collected for RNA and protein extraction.

Transcript expression analyses

Total RNA was extracted from frozen muscle using the SV Total RNA Isolation System (Promega). Deoxyribonuclease-treated RNA was reverse-transcribed using the iScript cDNA synthesis kit (Bio-Rad) and amplified with the Power SYBR Green Master Mix (Applied Biosystems). Data were analyzed using StepOne software and normalized to β-*actin* expression and relative to expression in control mice. The primers are listed in table S3.

Protein translation analysis

EDL muscles were powdered on dry ice before lysis in cold pull-down buffer [20 mM Hepes (pH 7.4), 50 mM KCl, 0.2 mM EDTA, 25 mM β-glycerophosphate, 0.5 mM Na-orthovanadate, 1 mM dithiothreitol, 0.5% Triton X-100, and 50 mM NaF] supplemented with complete protease inhibitor cocktail (Roche). Cells were disrupted by additional homogenization in a Potter homogenizer and 10-min incubation on ice before centrifugation for 10 min at 10,000 rpm at 4°C. Total protein concentration was determined (BCA Protein Assay, Pierce), and 200 μg of total lysate was used for m7GTP pull-down assay. After preclearing of the samples with glutathione-Sepharose beads (GE Healthcare, Amersham Biosciences) for 30 min at 4°C, 15 μl of a 50% slurry of m7GTP-Sepharose CL-4B (GE Healthcare, Amersham Biosciences) was incubated with the precleared supernatant for 4 hours at 4°C on a rotating wheel. After four washes, the samples were denaturized for 10 min at 95°C before separation on a gradient SDS polyacrylamide gel (3 to 12%; Novex). Eukaryotic translation initiation factor 4E (eIF4E) and eIF4E-binding protein 1 (4E-BP1) abundances on the m7GTP mimicking cap were quantified by chemiluminescence detection onto a nitrocellulose membrane.

Protein oxidation measurement

The extent of oxidation of residues in protein lysates was determined with the Oxyblot detection kit according to the manufacturer's protocol (Millipore). Total protein extract was used in duplicate and subjected to derivatization of protein carbonyl groups in the presence of 2.4-dinitrophenylhydrazine or not (control) for 15 min at room temperature. After neutralization of the reaction, the samples were reduced by the addition of 2-mercaptoethanol and boiled for 10 min at 95°C before separation on a gradient SDS polyacrylamide gel (3 to 12%; Novex). Upon transfer onto nitrocellulose membranes, detection of modified proteins was achieved with a rabbit anti-dinitrophenyl antibody (Millipore) and a secondary anti-rabbit horseradish peroxidase (HRP) antibody. Signal intensity was quantified and normalized to total protein amount after Ponceau staining of the nitrocellulose membranes.

Western blotting

TA muscles, WAT, BAT, liver, and pancreas were frozen in liquid nitrogen and pulverized on dry ice. They were lysed in cold radioimmunoprecipitation assay buffer [50 mM tris-HCl (pH 8), 150 mM NaCl, 1% NP-40, 0.5% sodium deoxycholate, 0.1% SDS] supplemented with protease inhibitor and phosphatase inhibitor cocktail tablets (Roche). Cell lysates were incubated on ice for 2 hours, sonicated two times for 15 s, and centrifuged at 13,600*g* for 20 min at 4°C. Cleared lysates were used to determine total protein amount (BCA Protein Assay, Pierce). Proteins were separated in 7 to 15% SDS polyacrylamide gels and transferred onto nitrocellulose membranes. Blood FGF21 analysis was performed on immunodepleted plasma using the ProteoPrep 20 Immunodepletion Kit (Sigma-Aldrich). HRP-conjugated secondary antibodies were used, and chemiluminescence was detected with the LumiGLO chemiluminiscent substrate system (KPL). Signal was captured on a Fusion Fx machine (VilberLourmat) and analyzed with FUSION Capt FX software. The following antibodies were used for immunoblotting or immunohistochemistry: phospho-AMPK Ser^{173} (#2535), AMPK (#2532), PGC1α (#2178), phospho-HSL Ser^{660} (#4126), β-actin (#4970), phospho-GSK3β Ser^{9} (#9322), GSK3β (#9315), phospho-GS Ser^{641} (#3891), GS (#3886), phospho-Akt Ser^{473} (#4058), phospho-AS160 Thr^{642} (#8881), AS160 (#2670), eEF2 (#2232), Ulk1 (#8054), phospho-PERK Thr^{980} (#3179), PERK (#3192), phospho-eIF2α Ser^{51} (#9721), eIF2α (#9722), S6 (#2217), phospho-eIF4E Ser^{209} (#9741), and 4E-BP1 (#9452) from Cell Signaling; PDK4 (sc-130841), CPT-1 (sc-20670), GLUT4 (sc-7938), GLUT1 (sc-7903), and ATF4 (sc-200) from Santa Cruz Biotechnology; α-actinin (7732) from Sigma; FGF21 (#Q9JJN1)

from R&D Systems; p62 (GP62-C) from Progen; and dinitrophenyl (MAB2223) from Millipore.

Histology and electron microscopy

Muscle, liver, and pancreas were dissected and frozen in nitrogen-cooled isopentane. Ten-micrometer sections were cut using a Cryostat (Leica CM1950). Inguinal subcutaneous WAT and BAT were dissected and fixed overnight in 4% paraformaldehyde. Samples were embedded in paraffin (Thermo Electron Corporation), and 4-μm-thick sections were cut using a microtome (Microm HM 360). The sections were stained with H&E according to classical methods. Light microscopy observations were performed using an upright microscope (DMR, Leica), and pictures were captured using a monochrome camera (DS-Ri1, Nikon). Transmission electron microscopy was performed as described elsewhere (*71*).

Statistical analyses

Results are expressed as means ± SEM of independent animals, with n (number of individual experiments) ≥3. Statistical comparison of two conditions was performed using Student's t test; comparison of three or more groups was performed using the one-way or two-way analysis of variance (ANOVA) test with Tukey correction for multiple comparisons; and analysis of normalized data or data sets where time is a variable was done using the linear regression model (GraphPad Prism Software). A confidence level of 0.05 was accepted for statistical significance.

SUPPLEMENTARY MATERIALS

www.sciencesignaling.org/cgi/content/full/8/402/ra113/DC1

Fig. S1. TSCmKO mice do not show overt behavioral changes.

Fig. S2. Higher plasma concentrations of free fatty acids in TSCmKO mice.

Fig. S3. TSCmKO mice do not show changes in the expression of genes encoding enzymes involved in glycolysis.

Fig. S4. FGF21 abundance in muscle is increased in TSCmKO mice.

Fig. S5. FGF21 in TSCmKO mice is not induced upon autophagy impairment or mitochondrial dysfunction.

Fig. S6. FGF21 blockade does not alter plasma insulin concentration in TSCmKO mice or metabolism in control mice.

Table S1. Weight and size analysis in 10- and 40-week-old mice.

Table S2. COBAS plasma analysis of 10-week-old mice.

Table S3. Primers used for quantitative polymerase chain reaction.

REFERENCES AND NOTES

1. R. A. DeFronzo, D. Tripathy, Skeletal muscle insulin resistance is the primary defect in type 2 diabetes. *Diabetes Care* **32** (Suppl. 2), S157–S163 (2009).
2. E. Llagostera, D. Catalucci, L. Marti, M. Liesa, M. Camps, T. P. Ciaraldi, R. Kondo, S. Reddy, W. H. Dillmann, M. Palacin, A. Zorzano, P. Ruiz-Lozano, R. Gomis, P. Kaliman, Role of myotonic dystrophy protein kinase (DMPK) in glucose homeostasis and muscle insulin action. *PLOS One* **2**, e1134 (2007).
3. B. K. Pedersen, M. A. Febbraio, Muscles, exercise and obesity: Skeletal muscle as a secretory organ. *Nat. Rev. Endocrinol.* **8**, 457–465 (2012).
4. K. H. Kim, Y. T. Jeong, H. Oh, S. H. Kim, J. M. Cho, Y.-N. Kim, S. S. Kim, D. H. Kim, K. Y. Hur, H. K. Kim, T. Ko, J. Han, H. L. Kim, J. Kim, S. H. Back, M. Komatsu, H. Chen, D. C. Chan, M. Konishi, N. Itoh, C. S. Choi, M.-S. Lee, Autophagy deficiency leads to protection from obesity and insulin resistance by inducing Fgf21 as a mitokine. *Nat. Med.* **19**, 83–92 (2013).
5. B. Angelin, T. E. Larsson, M. Rudling, Circulating fibroblast growth factors as metabolic regulators—A critical appraisal. *Cell Metab.* **16**, 693–705 (2012).
6. G. Gaich, J. Y. Chien, H. Fu, L. C. Glass, M. A. Deeg, W. L. Holland, A. Kharitonenkov, T. Bumol, H. K. Schilske, D. E. Moller, The effects of LY2405319, an FGF21 analog, in obese human subjects with type 2 diabetes. *Cell Metab.* **18**, 333–340 (2013).
7. T. Inagaki, P. Dutchak, G. Zhao, X. Ding, L. Gautron, V. Parameswara, Y. Li, R. Goetz, M. Mohammadi, V. Esser, J. K. Elmquist, R. D. Gerard, S. C. Burgess, R. E. Hammer, D. J. Mangelsdorf, S. A. Kliewer, Endocrine regulation of the fasting response by PPARα-mediated induction of fibroblast growth factor 21. *Cell Metab.* **5**, 415–425 (2007).
8. A. Kharitonenkov, T. L. Shiyanova, A. Koester, A. M. Ford, R. Micanovic, E. J. Galbreath, G. E. Sandusky, L. J. Hammond, J. S. Moyers, R. A. Owens, J. Gromada, J. T. Brozinick, E. D. Hawkins, V. J. Wroblewski, D.-S. Li, F. Mehrbod, S. R. Jaskunas, A. B. Shanafelt, FGF-21 as a novel metabolic regulator. *J. Clin. Invest.* **115**, 1627–1635 (2005).
9. J. Xu, D. J. Lloyd, C. Hale, S. Stanislaus, M. Chen, G. Sivits, S. Vonderfecht, R. Hecht, Y. S. Li, R. A. Lindberg, J. L. Chen, D. Y. Jung, Z. Zhang, H. J. Ko, J. K. Kim, M. M. Véniant, Fibroblast growth factor 21 reverses hepatic steatosis, increases energy expenditure, and improves insulin sensitivity in diet-induced obese mice. *Diabetes* **58**, 250–259 (2009).
10. W. L. Holland, A. C. Adams, J. T. Brozinick, H. H. Bui, Y. Miyauchi, C. M. Kusminski, S. M. Bauer, M. Wade, E. Singhal, C. C. Cheng, K. Volk, M.-S. Kuo, R. Gordillo, A. Kharitonenkov, P. E. Scherer, An FGF21-adiponectin-ceramide axis controls energy expenditure and insulin action in mice. *Cell Metab.* **17**, 790–797 (2013).
11. M. K. Badman, P. Pissios, A. R. Kennedy, G. Koukos, J. S. Flier, E. Maratos-Flier, Hepatic fibroblast growth factor 21 is regulated by PPARα and is a key mediator of hepatic lipid metabolism in ketotic states. *Cell Metab.* **5**, 426–437 (2007).
12. H. Wang, L. Qiang, S. R. Farmer, Identification of a domain within peroxisome proliferator-activated receptor γ regulating expression of a group of genes containing fibroblast growth factor 21 that are selectively repressed by SIRT1 in adipocytes. *Mol. Cell. Biol.* **28**, 188–200 (2008).
13. S. Keipert, M. Ost, K. Johann, F. Imber, M. Jastroch, E. M. van Schothorst, J. Keijer, S. Klaus, Skeletal muscle mitochondrial uncoupling drives endocrine cross-talk through the induction of FGF21 as a myokine. *Am. J. Physiol. Endocrinol. Metab.* **306**, E469–E482 (2014).
14. M. Laplante, D. M. Sabatini, mTOR signaling in growth control and disease. *Cell* **149**, 274–293 (2012).
15. P. Polak, N. Cybulski, J. N. Feige, J. Auwerx, M. A. Rüegg, M. N. Hall, Adipose-specific knockout of *raptor* results in lean mice with enhanced mitochondrial respiration. *Cell Metab.* **8**, 399–410 (2008).
16. A. Hagiwara, M. Cornu, N. Cybulski, P. Polak, C. Betz, F. Trapani, L. Terracciano, M. H. Heim, M. A. Rüegg, M. N. Hall, Hepatic mTORC2 activates glycolysis and lipogenesis through Akt, glucokinase, and SREBP1c. *Cell Metab.* **15**, 725–738 (2012).
17. C. F. Bentzinger, K. Romanino, D. Cloëtta, S. Lin, J. B. Mascarenhas, F. Oliveri, J. Xia, E. Casanova, C. F. Costa, M. Brink, F. Zorzato, M. N. Hall, M. A. Rüegg, Skeletal muscle-specific ablation of *raptor*, but not of *rictor*, causes metabolic changes and results in muscle dystrophy. *Cell Metab.* **8**, 411–424 (2008).
18. P. Castets, S. Lin, N. Rion, S. Di Fulvio, K. Romanino, M. Guridi, S. Frank, L. A. Tintignac, M. Sinnreich, M. A. Rüegg, Sustained activation of mTORC1 in skeletal muscle inhibits constitutive and starvation-induced autophagy and causes a severe, late-onset myopathy. *Cell Metab.* **17**, 731–744 (2013).
19. C. F. Bentzinger, S. Lin, K. Romanino, P. Castets, M. Guridi, S. Summermatter, C. Handschin, L. A. Tintignac, M. N. Hall, M. A. Rüegg, Differential response of skeletal muscles to mTORC1 signaling during atrophy and hypertrophy. *Skelet. Muscle* **3**, 6 (2013).
20. V. Risson, L. Mazelin, M. Roceri, H. Sanchez, V. Moncollin, C. Corneloup, H. Richard-Bulteau, A. Vignaud, D. Baas, A. Defour, D. Freyssenet, J.-F. Tanti, Y. Le-Marchand-Brustel, B. Ferrier, A. Conjard-Duplany, K. Romanino, S. Bauché, D. Hantai, M. Mueller, S. C. Kozma, G. Thomas, M. A. Rüegg, A. Ferry, M. Pende, X. Bigard, N. Koulmann, L. Schaeffer, Y.-G. Gangloff, Muscle inactivation of mTOR causes metabolic and dystrophin defects leading to severe myopathy. *J. Cell Biol.* **187**, 859–874 (2009).
21. D. LeRoith, S. Yakar, Mechanisms of disease: Metabolic effects of growth hormone and insulin-like growth factor 1. *Nat. Clin. Pract. End. Met.* **3**, 302–310 (2007).
22. P. Puigserver, Tissue-specific regulation of metabolic pathways through the transcriptional coactivator PGC1-α. *Int. J. Obes.* **29** (Suppl. 1), S5–S9 (2005).
23. Z. Wu, P. Puigserver, U. Andersson, C. Zhang, G. Adelmant, V. Mootha, A. Troy, S. Cinti, B. Lowell, R. C. Scarpulla, B. M. Spiegelman, Mechanisms controlling mitochondrial biogenesis and respiration through the thermogenic coactivator PGC-1. *Cell* **98**, 115–124 (1999).
24. J. C. Newman, E. Verdin, Ketone bodies as signaling metabolites. *Trends Endocrinol. Metab.* **25**, 42–52 (2014).
25. A. Bartelt, J. Heeren, Adipose tissue browning and metabolic health. *Nat. Rev. Endocrinol.* **10**, 24–36 (2014).
26. P. Seale, H. M. Conroe, J. Estall, S. Kajimura, A. Frontini, J. Ishibashi, P. Cohen, S. Cinti, B. M. Spiegelman, Prdm16 determines the thermogenic program of subcutaneous white adipose tissue in mice. *J. Clin. Invest.* **121**, 96–105 (2011).
27. H. Sano, S. Kane, E. Sano, C. P. Miinea, J. M. Asara, W. S. Lane, C. W. Garner, G. E. Lienhard, Insulin-stimulated phosphorylation of a Rab GTPase-activating protein regulates GLUT4 translocation. *J. Biol. Chem.* **278**, 14599 (2003).
28. S.-X. Tan, Y. Ng, J. G. Burchfield, G. Ramm, D. G. Lambright, J. Stöckli, D. E. James, The Rab GTPase-activating protein TBC1D4/AS160 contains an atypical phosphotyrosine-binding domain that interacts with plasma membrane phospholipids to facilitate GLUT4 trafficking in adipocytes. *Mol. Cell. Biol.* **32**, 4946–4959 (2012).
29. E. Hondares, M. Rosell, F. J. Gonzalez, M. Giralt, R. Iglesias, F. Villarroya, Hepatic FGF21 expression is induced at birth via PPARα in response to milk intake and contributes to thermogenic activation of neonatal brown fat. *Cell Metab.* **11**, 206–212 (2010).
30. C. L. Johnson, J. Y. Weston, S. A. Chadi, E. N. Fazio, M. W. Huff, A. Kharitonenkov, A. Köester, C. L. Pin, Fibroblast growth factor 21 reduces the severity of cerulein-induced pancreatitis in mice. *Gastroenterology* **137**, 1795–1804 (2009).
31. Y. Izumiya, H. A. Bina, N. Ouchi, Y. Akasaki, A. Kharitonenkov, K. Walsh, FGF21 is an Akt-regulated myokine. *FEBS Lett.* **582**, 3805–3810 (2008).
32. X. Ding, J. Boney-Montoya, B. M. Owen, A. L. Bookout, K. C. Coate, D. J. Mangelsdorf, S. A. Kliewer, βKlotho is required for fibroblast growth factor 21 effects on growth and metabolism. *Cell Metab.* **16**, 387–393 (2012).

33. H. P. Harding, I. Novoa, Y. Zhang, H. Zeng, R. Wek, M. Schapira, D. Ron, Regulated translation initiation controls stress-induced gene expression in mammalian cells. *Mol. Cell* **6**, 1099–1108 (2000).
34. S. Varadarajan, E. T. Bampton, J. L. Smalley, K. Tanaka, R. E. Caves, M. Butterworth, J. Wei, M. Pellecchia, J. Mitcheson, T. W. Gant, D. Dinsdale, G. M. Cohen, A novel cellular stress response characterised by a rapid reorganisation of membranes of the endoplasmic reticulum. *Cell Death Differ.* **19**, 1896–1907 (2012).
35. I. Kim, W. Xu, J. C. Reed, Cell death and endoplasmic reticulum stress: Disease relevance and therapeutic opportunities. *Nat. Rev. Drug Discov.* **7**, 1013–1030 (2008).
36. C. Hetz, The unfolded protein response: Controlling cell fate decisions under ER stress and beyond. *Nat. Rev. Mol. Cell Biol.* **13**, 89–102 (2012).
37. N. Ohoka, S. Yoshii, T. Hattori, K. Onozaki, H. Hayashi, *TRB3*, a novel ER stress-inducible gene, is induced via ATF4-CHOP pathway and is involved in cell death. *EMBO J.* **24**, 1243–1255 (2005).
38. C. Appenzeller-Herzog, M. N. Hall, Bidirectional crosstalk between endoplasmic reticulum stress and mTOR signaling. *Trends Cell Biol.* **22**, 274–282 (2012).
39. U. Özcan, E. Yilmaz, L. Özcan, M. Furuhashi, E. Vaillancourt, R. O. Smith, C. Z. GörgÜn, G. S. Hotamisligil, Chemical chaperones reduce ER stress and restore glucose homeostasis in a mouse model of type 2 diabetes. *Science* **313**, 1137–1140 (2006).
40. B. A. Omar, B. Andersen, J. Hald, K. Raun, E. Nishimura, B. Ahren, Fibroblast growth factor 21 (FGF21) and glucagon-like peptide 1 contribute to diabetes resistance in glucagon receptor-deficient mice. *Diabetes* **63**, 101–110 (2014).
41. F. M. Fisher, S. Kleiner, N. Douris, E. C. Fox, R. J. Mepani, F. Verdeguer, J. Wu, A. Kharitonenkov, J. S. Flier, E. Maratos-Flier, B. M. Spiegelman, FGF21 regulates PGC-1α and browning of white adipose tissues in adaptive thermogenesis. *Genes Dev.* **26**, 271–281 (2012).
42. J. L. Yecies, H. H. Zhang, S. Menon, S. Liu, D. Yecies, A. I. Lipovsky, C. Gorgun, D. J. Kwiatkowski, G. S. Hotamisligil, C.-H. Lee, B. D. Manning, Akt stimulates hepatic SREBP1c and lipogenesis through parallel mTORC1-dependent and independent pathways. *Cell Metab.* **14**, 21–32 (2011).
43. T. R. Peterson, S. S. Sengupta, T. E. Harris, A. E. Carmack, S. A. Kang, E. Balderas, D. A. Guertin, K. L. Madden, A. E. Carpenter, B. N. Finck, D. M. Sabatini, mTOR complex 1 regulates lipin 1 localization to control the SREBP pathway. *Cell* **146**, 408–420 (2011).
44. C. Xu, B. Bailly-Maitre, J. C. Reed, Endoplasmic reticulum stress: Cell life and death decisions. *J. Clin. Invest.* **115**, 2656–2664 (2005).
45. Z. Mounir, J. L. Krishnamoorthy, S. Wang, B. Papadopoulou, S. Campbell, W. J. Muller, M. Hatzoglou, A. E. Koromilas, Akt determines cell fate through inhibition of the PERK-eIF2α phosphorylation pathway. *Sci. Signal.* **4**, ra62 (2011).
46. A. C. Riggs, E. Bernal-Mizrachi, M. Ohsugi, J. Wasson, S. Fatrai, C. Welling, J. Murray, R. E. Schmidt, P. L. Herrera, M. A. Permutt, Mice conditionally lacking the Wolfram gene in pancreatic islet beta cells exhibit diabetes as a result of enhanced endoplasmic reticulum stress and apoptosis. *Diabetologia* **48**, 2313–2321 (2005).
47. M. Cornu, W. Oppliger, V. Albert, A. M. Robitaille, F. Trapani, L. Quagliata, T. Fuhrer, U. Sauer, L. Terracciano, M. N. Hall, Hepatic mTORC1 controls locomotor activity, body temperature, and lipid metabolism through FGF21. *Proc. Natl. Acad. Sci. U.S.A.* **111**, 11592–11599 (2014).
48. T. Iannitti, B. Palmieri, Clinical and experimental applications of sodium phenylbutyrate. *Drugs R D* **11**, 227–249 (2011).
49. A. L. Bookout, M. H. M. de Groot, B. M. Owen, S. Lee, L. Gautron, H. L. Lawrence, X. Ding, J. K. Elmquist, J. S. Takahashi, D. J. Mangelsdorf, S. A. Kliewer, FGF21 regulates metabolism and circadian behavior by acting on the nervous system. *Nat. Med.* **19**, 1147–1152 (2013).
50. W. Wei, P. A. Dutchak, X. Wang, X. Ding, X. Wang, A. L. Bookout, R. Goetz, M. Mohammadi, R. D. Gerard, P. C. Dechow, D. J. Mangelsdorf, S. A. Kliewer, Y. Wan, Fibroblast growth factor 21 promotes bone loss by potentiating the effects of peroxisome proliferator-activated receptor γ. *Proc. Natl. Acad. Sci. U.S.A.* **109**, 3143–3148 (2012).
51. M. J. Potthoff, T. Inagaki, S. Satapati, X. Ding, T. He, R. Goetz, M. Mohammadi, B. N. Finck, D. J. Mangelsdorf, S. A. Kliewer, S. C. Burgess, FGF21 induces PGC-1α and regulates carbohydrate and fatty acid metabolism during the adaptive starvation response. *Proc. Natl. Acad. Sci. U.S.A.* **106**, 10853–10858 (2009).
52. C. Wang, J. Dai, M. Yang, G. Deng, S. Xu, Y. Jia, G. Boden, Z. A. Ma, G. Yang, L. Li, Silencing of FGF-21 expression promotes hepatic gluconeogenesis and glycogenolysis by regulation of the STAT3-SOCS3 signal. *FEBS J.* **281**, 2136–2147 (2014).
53. E. D. Berglund, C. Y. Li, H. A. Bina, S. E. Lynes, M. D. Michael, A. B. Shanafelt, A. Kharitonenkov, D. H. Wasserman, Fibroblast growth factor 21 controls glycemia via regulation of hepatic glucose flux and insulin sensitivity. *Endocrinology* **150**, 4084–4093 (2009).
54. K. Inoki, T. Zhu, K.-L. Guan, TSC2 mediates cellular energy response to control cell growth and survival. *Cell* **115**, 577–590 (2003).
55. R. M. Young, D. Ackerman, Z. L. Quinn, A. Mancuso, M. Gruber, L. Liu, D. N. Giannoukos, E. Bobrovnikova-Marjon, J. A. Diehl, B. Keith, M. C. Simon, Dysregulated mTORC1 renders cells critically dependent on desaturated lipids for survival under tumor-like stress. *Genes Dev.* **27**, 1115–1131 (2013).
56. K. R. Markan, M. C. Naber, M. K. Ameka, M. D. Anderegg, D. J. Mangelsdorf, S. A. Kliewer, M. Mohammadi, M. J. Potthoff, Circulating FGF21 is liver derived and enhances glucose uptake during refeeding and overfeeding. *Diabetes* **63**, 4057–4063 (2014).
57. P. Domingo, J. M. Gallego-Escuredo, J. C. Domingo, M. Gutiérrez Mdel, M. G. Mateo, I. Fernández, F. Vidal, M. Giralt, F. Villarroya, Serum FGF21 levels are elevated in association with lipodystrophy, insulin resistance and biomarkers of liver injury in HIV-1-infected patients. *Aids* **24**, 2629–2637 (2010).
58. B. Lindegaard, T. Hvid, T. Grondahl, C. Frosig, J. Gerstoft, P. Hojman, B. K. Pedersen, Expression of fibroblast growth factor-21 in muscle is associated with lipodystrophy, insulin resistance and lipid disturbances in patients with HIV. *PLOS One* **8**, e55632 (2013).
59. Y. Zhang, Y. Xie, E. D. Berglund, K. C. Coate, T. T. He, T. Katafuchi, G. Xiao, M. J. Potthoff, W. Wei, Y. Wan, R. T. Yu, R. M. Evans, S. A. Kliewer, D. J. Mangelsdorf, The starvation hormone, fibroblast growth factor-21, extends lifespan in mice. *Elife* **1**, e00065 (2012).
60. T. Inagaki, V. Y. Lin, R. Goetz, M. Mohammadi, D. J. Mangelsdorf, S. A. Kliewer, Inhibition of growth hormone signaling by the fasting-induced hormone FGF21. *Cell Metab.* **8**, 77–83 (2008).
61. S. Wu, T. Grunwald, A. Kharitonenkov, J. Dam, R. Jockers, F. De Luca, Increased expression of fibroblast growth factor 21 (FGF21) during chronic undernutrition causes growth hormone insensitivity in chondrocytes by inducing leptin receptor overlapping transcript (LEPROT) and leptin receptor overlapping transcript-like 1 (LEPROTL1) expression. *J. Biol. Chem.* **288**, 27375–27383 (2013).
62. B. M. Owen, A. L. Bookout, X. Ding, V. Y. Lin, S. D. Atkin, L. Gautron, S. A. Kliewer, D. J. Mangelsdorf, FGF21 contributes to neuroendocrine control of female reproduction. *Nat. Med.* **19**, 1153–1156 (2013).
63. F. J. Ramos, S. C. Chen, M. G. Garelick, D.-F. Dai, C.-Y. Liao, K. H. Schreiber, V. L. MacKay, E. H. An, R. Strong, W. C. Ladiges, P. S. Rabinovitch, M. Kaeberlein, B. K. Kennedy, Rapamycin reverses elevated mTORC1 signaling in lamin A/C-deficient mice, rescues cardiac and skeletal muscle function, and extends survival. *Sci. Transl. Med.* **4**, 144ra103 (2012).
64. P. Spitali, P. Grumati, M. Hiller, M. Chrisam, A. Aartsma-Rus, P. Bonaldo, Autophagy is impaired in the tibialis anterior of dystrophin null mice. *PLOS Curr.* 10.1371/currents.md.e1226cefa851a2f079bbc406c0a21e80 (2013).
65. D. J. Kwiatkowski, H. Zhang, J. L. Bandura, K. M. Heiberger, M. Glogauer, N. el-Hashemite, H. Onda, A mouse model of TSC1 reveals sex-dependent lethality from liver hemangiomas, and up-regulation of p70S6 kinase activity in Tsc1 null cells. *Hum. Mol. Genet.* **11**, 525–534 (2002).
66. S. C. Bodine, T. N. Stitt, M. Gonzalez, W. O. Kline, G. L. Stover, R. Bauerlein, E. Zlotchenko, A. Scrimgeour, J. C. Lawrence, D. J. Glass, G. D. Yancopoulos, Akt/mTOR pathway is a crucial regulator of skeletal muscle hypertrophy and can prevent muscle atrophy in vivo. *Nat. Cell Biol.* **3**, 1014–1019 (2001).
67. O. P. McGuinness, J. E. Ayala, M. R. Laughlin, D. H. Wasserman, NIH experiment in centralized mouse phenotyping: The Vanderbilt experience and recommendations for evaluating glucose homeostasis in the mouse. *Am. J. Physiol. Endocrinol. Metab.* **297**, E849–E855 (2009).
68. A. Joseph, K. Neff, J. Richard, L. Gao, D. Bangari, M. Joly, K. Culm-Merdek, R. Garman, J. Williams, S. Richards, M. Ruzek, Transient low-dose methotrexate induces tolerance to murine anti-thymocyte globulin and together they promote long-term allograft survival. *J. Immunol.* **189**, 732–743 (2012).
69. K. Saito, S. Lee, T. Shiuchi, C. Toda, M. Kamijo, K. Inagaki-Ohara, S. Okamoto, Y. Minokoshi, An enzymatic photometric assay for 2-deoxyglucose uptake in insulin-responsive tissues and 3T3-L1 adipocytes. *Anal. Biochem.* **412**, 9–17 (2011).
70. X. C. Kong, P. Barzaghi, M. A. Ruegg, Inhibition of synapse assembly in mammalian muscle in vivo by RNA interference. *EMBO Rep.* **5**, 183–188 (2004).
71. J. Moll, P. Barzaghi, S. Lin, G. Bezakova, H. Lochmüller, E. Engvall, U. Müller, M. A. Ruegg, An agrin minigene rescues dystrophic symptoms in a mouse model for congenital muscular dystrophy. *Nature* **413**, 302–307 (2001).

Acknowledgments: We thank C. Handschin for his remarks on the manuscript and K. Romanino, M. Kaiser, F. Olivieri, M. Cornu, V. Albert, M. Beer, and K. Svensson for technical assistance. **Funding:** This work was supported by the Cantons of Basel-Stadt and Basel-Land and by grants from the Swiss National Science Foundation and the Swiss Foundation for Research on Muscle Disease. **Author contributions:** M.G. designed and performed most of the experiments, analyzed the data, and wrote the paper; L.A.T. collaborated on the experimental design, performed protein oxidation and translation experiments, supervised the project, and wrote the paper; S.L. collaborated on the electroporation experiments and tissue dissection; B.K. collaborated on the glucose homeostasis experiments and the CLAMS experiments; P.C. collaborated on the autophagy-related Western blot analysis and wrote the paper; M.A.R. designed the experiments, supervised the entire project, and wrote the paper. All authors contributed and commented on the manuscript. **Competing interests:** The authors declare that they have no competing interests.

Submitted 17 April 2015
Accepted 22 October 2015
Final Publication 10 November 2015
10.1126/scisignal.aab3715
Citation: M. Guridi, L. A. Tintignac, S. Lin, B. Kupr, P. Castets, M. A. Rüegg, Activation of mTORC1 in skeletal muscle regulates whole-body metabolism through FGF21. *Sci. Signal.* **8**, ra113 (2015).

Activation of mTORC1 in skeletal muscle regulates whole-body metabolism through FGF21

Maitea Guridi, Lionel A. Tintignac, Shuo Lin, Barbara Kupr, Perrine Castets and Markus A. Rüegg (November 10, 2015)

Science Signaling **8** (402), ra113. [doi: 10.1126/scisignal.aab3715]

Science Signaling (ISSN 1937-9145) is published weekly, except the last December, by the American Association for the Advancement of Science, 1200 New York Avenue, NW, Washington, DC 20005.